Vortex Dynamics Models in Flow Control Problems

B Protas

Department of Mathematics and Statistics, McMaster University, Hamilton, Ontario L8S 4K1, Canada

E-mail: bprotas@mcmaster.ca

Abstract. In this paper we review the state of the art in the field of control of vortex dynamics. We focus on problems governed by two–dimensional incompressible Euler equations in domains both with and without boundaries. Following a comprehensive review of earlier approaches, we discuss how methods of modern control and optimization theory can be employed to solve control problems for vortex system. In addition, we also address the companion problem of the state estimation for vortex systems. While most of the discussion concerns point vortex systems, in the second part of the paper we also introduce a novel approach to the control of Euler flows involving finite–area vorticity distributions. The paper concludes with what, in the author's opinion, represent promising new research directions.

PACS numbers: 47.32.C-, 47.85.L-, 47.15.Ki

1. Introduction

The goal of this article is to review the recent progress and address some open questions in the area of control of vortex–dominated flows. This article is written from the interdisciplinary perspective grounded in the theoretical fluid dynamics and straddling the fields of the control and optimization theory. We will first clarify what we mean by "control" problems. Let us consider a system characterized by a state variable $\mathbf{X}$, either finite–dimensional or infinite–dimensional, and depending on time t and some input (control) variable $\mathbf{U}$, i.e., $\mathbf{X} = \mathbf{X}(t, \mathbf{U})$. We will also assume that the system evolution is governed by a differential equation $\mathbf{E}(\mathbf{X}, \mathbf{U}) = \mathbf{0}$ with suitable initial conditions. The control problem can thus be stated as follows:

Problem 1 (control) *Given an initial state* $\mathbf{X}_1 = \mathbf{X}(0)$ *of the system and a prescribed final state* $\mathbf{X}_2 = \mathbf{X}(T)$*, determine the control* $\mathbf{U}$ *that will move the system from* $\mathbf{X}_1$ *to* $\mathbf{X}_2$ *during the time interval* $[0, T]$.

We refer the reader to the monograph by Sontag [1] for a modern account of the theory of control, and to [2] for a historical overview. A related problem concerns system "optimization" and can be stated thus:

Problem 2 (optimization) *Find the optimal input parameters* $\mathbf{U}^{opt}$ *and the corresponding optimal state* $\mathbf{X}^{opt}$ *which extremize a measure of the system performance expressed mathematically by the function* $j = j(\mathbf{X}, \mathbf{U})$*, i.e.,*

$$\begin{aligned} &(\mathbf{X}^{opt}, \mathbf{U}^{opt}) = \mathrm{argmin}_{\mathbf{X},\mathbf{U}}\, j(\mathbf{X}, \mathbf{U}), \\ &\textit{subject to}\ \ \mathbf{E}(\mathbf{X}, \mathbf{U}) = \mathbf{0} \end{aligned} \tag{1}$$

(the function "argmin" returns the values of the arguments $\mathbf{X}$ and $\mathbf{U}$ for which $j(\mathbf{X}, \mathbf{U})$ attains a minimum). The foundations of the modern theory of optimization were laid by Kantorovich and Dantzig (for which the former was honored with the Nobel Prize in Economics in 1975), and developed further by many scholars. A modern account of this field can be found in the monographs [3, 4, 5]. At an intersection of the optimization and control theory one finds the field of "optimal control" where one seeks to solve Problem 1 in an optimal way, i.e., by requiring the control $\mathbf{U}$ to extremize some performance criterion as in Problem 2. Following earlier related developments in the calculus of variations, the field of modern optimal control theory originated with the work of Pontryagin [6]; we refer the reader to the monograph [7] for an up–to–date account of this field. In general, solution of such problems usually involves an *open–loop* control $\mathbf{U}$ which depends on the initial and final states of the system as well as the time. An important subclass of control problems are *stabilization* problems defined as follows:

Problem 3 (stabilization) *Consider a system governed by an equation* $\mathbf{E}_w(\mathbf{X}, \mathbf{U}, \mathbf{W}) = \mathbf{0}$*, where* $\mathbf{W}$ *represents stochastic inputs. Determine a control input* $\mathbf{U}$ *that will contain the state* $\mathbf{X}$ *of the system in a neighborhood of some solution* $\mathbf{X}_0$*, either time–dependent or steady, of the deterministic problem* $\mathbf{E}(\mathbf{X}_0, \mathbf{U}) = \mathbf{E}_w(\mathbf{X}_0, \mathbf{U}, \mathbf{0}) = \mathbf{0}$.

The solution of stabilization problems usually involves *closed–loop* (*feedback*) control which depends on the instantaneous state of the system only, i.e., $\mathbf{U} = \mathbf{U}(\mathbf{X})$. In practice, optimal

control and stabilization problems sometimes occur together, namely, when systems actuated with optimal open–loop controls require additional stabilization in order to reject exogenous disturbances and in this way to achieve robustness. Another class of problems which can also be cast as optimal control problems are state estimation problems defined thus:

Problem 4 (estimation) *Reconstruct the state* $\mathbf{X}$ *of the system given its incomplete and noisy measurements* $\tilde{\mathbf{Y}}$.

A common feature of Problems 1–4 is that they represent *inverse problems* in which, instead of merely looking for solutions of a system of equations $\mathbf{E}(\mathbf{X},\mathbf{U}) = \mathbf{0}$, one looks for input parameters $\mathbf{U}$ such that the solution $\mathbf{X}$ has some desired properties. The study of a control problem usually involves two stages: *analysis* of the control system seeks to identify conditions under which Problems 1–4 can be solved and often requires an examination of the *controllability* and *observability* of the system; *synthesis* of the control is the subsequent phase during which the actual control is determined. A discussion of all relevant details of problems 1–4 would take us far outside the scope of this paper. Therefore, when surveying different results, we will usually emphasize the new concepts and refer the reader to the control–theoretic literature for details.

During the last 15 years or so the state–of–the–art computational fluid dynamics (CFD) on the one hand, and control methods for Problem 1–4 on the other hand, both reached a degree of computational efficiency which made it possible to start to tackle realistic problems of flow control in a systematic manner. While in principle the control theory for infinite–dimensional systems described by partial differential equations (PDEs) is, at least in the linear setting, relatively well understood [8, 9], actual computational solution of such problems still remains very difficult. Despite several remarkable successes (see the monographs [10, 11] and the survey articles [12, 13, 14] for a broad and up–to–date perspective), solution of many real–life problems continues to present formidable challenges. They are mostly related to the computational resources, both in terms of the CPU time and storage, required to obtain the solution: for example, solution of Problem 2 for a time–dependent system often requires as many as $O(10^1 - 10^2)$ solutions of the system of governing equations over the time–window of interest. On the other hand, determination of the feedback kernels needed in the "simplest" solutions to Problems 3 and 4 requires the solution of a discretized operator equation with $O(N^2)$ variables, where N is the number of the computational degrees of freedom in the discretization of the flow problem. Despite the steady increase of the computational power available, these limitations will at least for some time remain prohibitive when it comes to solution of control problems for high–Reynolds number flows in nontrivial domains. This realization has motivated the pursuit of various simplifying approaches that, by reducing significantly the number of the relevant degrees of freedom, render solution of such control problems feasible. The first of the two main trends relies on the use of the truncated Galerkin bases with small dimensions. Such bases, which are designed to optimally capture the system evolution in the energy norm, can be constructed using the proper orthogonal decomposition (POD) techniques [15]. POD–based approaches to solution of flow control problems are currently the subject of active research [16, 17]. The second of these trends

relies on a simplification of the mathematical model of the problem by neglecting the effects considered less important in a given setting. For instance, a family of amplitude equations, known as the Landau–Ginzburg models, have been quite successful describing the onset and development of various hydrodynamics instabilities [18], and control of such model problems was investigated in [20, 19, 21, 22]. Another such possibility is to neglect the viscous diffusion which is equivalent to using the Euler equation instead of the Navier–Stokes equation as the mathematical model of the flow problem. It is particularly relevant to high–Reynolds number phenomena dominated by nonlinear "vortex dynamics", i.e., the dynamics of localized vortical structures embedded in a quasi–irrotational flow. Such vortex–based approaches to solution of flow control problem are currently also the subject of active research, and the purpose of the present article is to review the recent advances in this area. An earlier review of this field was written by Vainchtein and Mezić [23].

The concept of the vortex dynamics in its modern sense goes back to the seminal paper by Helmholtz [24]. Since the year 1858 when it was published, the theory of vortex motion has been elaborated by many eminent scholars. Instead of attempting to review this immense body of work, we refer the reader to the monograph by Truesdell [25] which contains many bibliographical references and the recently published bibliography collected by Meleshko and Aref [26] which, to the author's best knowledge, is the most comprehensive resource available as regards the literature on this topic published until the middle of the 20th century. Vortex motion was also discussed at length in many classical textbooks on the theoretical fluid dynamics including [27, 28, 29, 30, 31] in addition to modern monographs [32, 33] and review papers [34, 35]. This subject was also treated from the point of view of the modern mathematical analysis in [36, 37]. In the present paper we will primarily focus on vortex systems as "models" of fluid flow, however, it should be emphasized that starting with the seminal work of Rosenhead [38], they have also given rise to the "vortex methods" [39], an autonomous family of numerical methods designed for the solution of a class of evolutionary PDEs.

It is well–known that certain important properties of the vortex motion in two–dimensional (2D) and three–dimensional (3D) flows can be quite different. However, since most of the control problems dealt in fact with vortex flows in 2D, this is the setting we will be concerned with in this article. We will assume $\Omega \subseteq \mathbb{R}^2$ to be our domain, either bounded or unbounded, with $\partial\Omega$ denoting its boundary, if it is present. Using the time–dependent streamfunction $\psi(t,\cdot) : \Omega \to \mathbb{R}$, the motion of the inviscid incompressible fluid is described by the Euler equation which can be written in the form [37]

$$\begin{cases} \dfrac{\partial \Delta\psi}{\partial t} + J(\Delta\psi,\psi) = 0 \qquad \text{in } \Omega \times (0,T], \\ \psi|_{\partial\Omega} = \psi_b, \\ \psi|_{t=0} = \psi_0, \end{cases} \tag{2}$$

where $J(f,g) \triangleq \frac{\partial f}{\partial x}\frac{\partial g}{\partial y} - \frac{\partial f}{\partial y}\frac{\partial g}{\partial x}$ is the Jacobian with $(x,y) \in \Omega$ (the symbol "$\triangleq$" means "equal to by definition"), $\Delta \triangleq \frac{\partial^2}{\partial x^2} + \frac{\partial^2}{\partial y^2}$ is the Laplacian operator, T is the length of the time interval we are interested in, whereas ψ_b and ψ_0 are, respectively, the boundary and initial conditions.

Given the streamfunction ψ as a solution of (2), the velocity field can be expressed as $\mathbf{u} = [u, v] = \left[\frac{\partial \psi}{\partial y}, -\frac{\partial \psi}{\partial x}\right]$ so that it satisfies by construction the incompressibility condition $\nabla \cdot \mathbf{u} = 0$. We remark that in view of the identity $-\frac{\partial \psi}{\partial \tau}\Big|_{\partial\Omega} \triangleq -\tau \cdot \nabla\psi\Big|_{\partial\Omega} = \mathbf{u} \cdot \mathbf{n}|_{\partial\Omega}$, where $\mathbf{n}$ and τ are, respectively, the outward facing normal and the associated tangent unit vectors on the boundary $\partial\Omega$, the boundary condition in (2) is in fact equivalent to prescribing the wall–normal velocity component‡. In the case of steady–state problems system (2) reduces to a nonlinear boundary–value problem [37], namely

$$\begin{cases} \Delta\psi = F(\psi) & \text{in } \Omega, \\ \psi|_{\partial\Omega} = \psi_b \end{cases} \tag{3}$$

where $F(\psi)$ is an arbitrary function. We emphasize that this non–determinacy of the function $F(\psi)$ is a signature of the lack of uniqueness of solutions of (3). Most control problems have been considered for a particular family of (weak) solutions of (2) and (3), namely, systems of *point vortices*, in which all the vorticity is concentrated in isolated singularities. In addition to reviewing these results, we will also present some novel ideas concerning the optimal control of another family of solutions of (2) and (3) which generalizes the concept of point vortices. These will be the *Prandtl–Batchelor flows* [40, 41] distinguished by the presence of vortex patches with constant vorticity.

Vortex models have been employed in a vast range of applications in science and engineering which it is impossible to review here. In order to fix attention and provide motivation for the subsequent discussion of some idealized cases, we mention here three specific applications that have received a lot of attention:

- modeling coherent structures in 2D turbulent flows [42], where some of the ideas are due to the seminal work of Onsager [43]; in addition to understanding the fundamental properties of 2D turbulence, such models found applications in the Geophysical Fluid Dynamics [44],
- modeling recirculation regions attached to objects such as bluff bodies and airfoils [45]; models of this type are relevant to the problem of lift enhancement via stabilization of trapped vortices in aeronautical applications [46],
- modeling generation of thrust in fish–like locomotion [47, 48, 49].

Over the years several different control techniques have been applied to vortex dynamics problems, many of which were based on ad–hoc and/or speculative arguments. While in our survey we will attempt to do justice to most noteworthy approaches, our focus will be primarily on techniques based on solid mathematical foundations. Therefore, our presentation will involve a blend of mathematical analysis and results of numerical computations.

The structure of the paper is as follows: in the next Section we state some basic facts concerning vortex motion in 2D domains with and without boundaries; in this Section we

‡ We remark that when Ω is *multiply*–connected, ψ_b is defined up to a constant on any closed boundary segment, and formulation (2) must be modified to account for the cyclic constants representing the circulations around the contours [27, 30, 31].

also analyze different vortex equilibria and their stability properties, next in the rather short Section 3 we discuss the control of vortex systems in domains without boundaries, whereas in Section 4 we will discuss it in the case of domains with boundaries where most of our attention will be on vortex flows past bodies§, then in Section 5 we will discuss the dual concept of the state estimation for vortex systems, whereas in Section 6 we will introduce some novel concepts concerning the optimal control of vortex flows with finite–area vorticity distributions, summary, conclusions and a discussion of some future research directions are deferred to Section 7.

2. Point Vortex Systems — Dynamics and Equilibria

In this Section we discuss the equations governing the motion of point vortices, first in unbounded, then in bounded, domains. Subsequently, we recast these equations into a formalism employed in the modern control theory [1, 7]. Finally, owing to their importance for stabilization problems, we discuss point vortex equilibria in flows past objects focusing on their stability.

2.1. Point Vortex Dynamics in Domains without Boundaries

Description of the vortex motion can be made more succinct using methods of the complex analysis and hereafter we will frequently employ this formalism. Identifying the position of a point vortex with a point in the complex plane, i.e., $z_1 = x_1 + \mathrm{i}y_1 \in \mathbb{C}$, where $\mathrm{i} = \sqrt{-1}$, and in view of the identity $\Delta\psi = -\omega$ [37], where ω is the vorticity, the complex potential $W(z)$ induced at a point $z \in \mathbb{C}$ by a point vortex located at z_1 in an unbounded domain is given in terms of complex Green's function for the Laplace equation, i.e.,

$$W(z) = \frac{\Gamma_1}{2\pi\mathrm{i}} \ln(z - z_1), \tag{4}$$

where Γ_1 is the circulation of the vortex. The complex velocity can then be obtained as

$$V(z) \triangleq (u - \mathrm{i}v)(z) = \frac{dW(z)}{dz} = \frac{\Gamma}{2\pi\mathrm{i}} \frac{1}{z - z_1}. \tag{5}$$

Assuming that there are N such vortices in the plane with the coordinates $z_k \in \mathbb{C}$, $k = 1, \ldots, N$ and circulations $\{\Gamma_k\}_{k=1}^N$, their evolution is governed by the following system of nonlinear complex differential equations (ODEs)

$$\frac{d\bar{z}_k}{dt} = \frac{1}{2\pi\mathrm{i}} {\sum_{l=1}^{N}}' \frac{\Gamma_l}{z_k - z_l}, \quad k = 1, \ldots, N, \tag{6}$$

where the overline denotes complex conjugation and the prime on the summation symbol indicates that the singular self–induction terms with $k = l$ are omitted. Separating the real and

§ Here we emphasize the distinction between bounded domains and domains with boundaries, as the latter may in general be unbounded, at least in some directions, but may possess some internal boundaries.

imaginary parts in (6) we obtain

$$\frac{dx_k}{dt} = -\frac{1}{2\pi}{\sum_{l=1}^{N}}' \frac{\Gamma_l(y_k - y_l)}{r_{kl}}, \tag{7a}$$

$$\frac{dy_k}{dt} = \frac{1}{2\pi}{\sum_{l=1}^{N}}' \frac{\Gamma_l(x_k - x_l)}{r_{kl}}, \quad k = 1,\ldots,N, \tag{7b}$$

where $r_{kl} \triangleq \sqrt{(x_k - x_l)^2 + (y_k - y_l)^2}$. System (7*a*)–(7*b*) is known to possess several remarkable properties [33]. For example, defining the Hamiltonian as

$$\mathcal{H} \triangleq -\frac{1}{4\pi}{\sum_{k,l=1}^{N}}' \Gamma_k \Gamma_l \ln r_{kl} \tag{8}$$

and defining the generalized coordinates and momenta respectively as $q_k \triangleq x_k$ and $p_k \triangleq \Gamma_k y_k$, $k = 1,\ldots,N$, (7*a*)–(7*b*) can be cast into the Hamiltonian form

$$\frac{dq_k}{dt} = \frac{\partial \mathcal{H}}{\partial p_k}, \tag{9a}$$

$$\frac{dp_k}{dt} = -\frac{\partial \mathcal{H}}{\partial q_k}, \quad k = 1,\ldots,N. \tag{9b}$$

In addition to the Hamiltonian $\mathcal{H}$, system (7*a*)–(7*b*) also conserves the two components of the linear impulse and the angular impulse. The Hamiltonian formalism can be made even more elegant using methods of the geometric mechanics [33]. N–vortex systems admit many different equilibria, including asymmetric states [50, 35]. As shown by Gröbli [51], see also [52], system (7*a*)–(7*b*) is integrable for $N \leq 3$ and is in general non–integrable for $N > 3$. Point vortex dynamics is an area of mathematical physics that has traditionally served as a "playground", to use the term recently employed by Aref [35], for methods stemming from fairly disparate areas of mathematics, both applied and pure.

2.2. Point Vortex Dynamics in Domains with Boundaries

In the presence of solid boundaries the most important complication stems from the fact that the evolution of system (6) is now constrained by the condition that the normal velocity component vanish on all solid boundaries $\mathbf{u}\cdot\mathbf{n}|_{\partial\Omega} = 0$, or equivalently $\psi|_{\partial\Omega} = \psi_b$. Arguably the most straightforward approach to satisfy this constraint is to use the "method of images" [27, 30] which treats solid boundaries as streamlines of a flow field defined in the entire complex plane $\mathbb{C}$ and then, for every point vortex present in Ω, uses suitably chosen images located in $\mathbb{C}\backslash\overline{\Omega}$. The location of these image vortices is geometry–dependent and is chosen to ensure that the normal velocity induced together by the original and image systems vanish everywhere on the boundary $\partial\Omega$. For example, for a vortex in the exterior of a cylinder with radius R the image vortices can be determined using the "circle theorem" [30] which states that if $\tilde{w}(z)$ is the complex potential of a flow in a domain without boundaries and with singularities at some points z_k such that $\forall_k$, $|z_k| > R$, then the complex potential of the corresponding flow past the cylinder is given by the expression $w(z) = \tilde{w}(z) + \overline{\tilde{w}}(\frac{R^2}{z})$. The second term in the expression for $w(z)$ represents "image singularities" located inside the obstacle.

Incorporation of nontrivial boundary conditions could also be done using other, more general, techniques applicable to the case when the vorticity distribution includes finite–area vortex regions and the domain boundaries have more complicated shapes. The method of images can be reformulated in terms of suitably modified Green's functions constructed to ensure that the boundary conditions are satisfied on all boundaries [30]. Using such modified Green's functions it is possible to generalize Hamiltonian formulation (8), (9*a*), (9*b*) for the case of vortex motion in bounded domains as was done by Lin [53] (the Hamiltonian $\mathcal{H}$ generalized for the case of bounded domains is often referred to as the Kirchhoff–Routh path function [32]). These results were recently brought to an implementable form by Crowdy and Marshall in [54] where methods of the classical function theory were used to derive explicit expressions for modified Green's functions. Yet another possibility to account for the presence of impermeable boundaries is by using a singular vorticity distribution on the boundary, a so–called "vortex sheet" [32]. While such techniques turn out to be quite useful in numerical computations [39], they are less tractable from the analytical point of view. In most examples discussed in this survey it is sufficient to use the method of images. Needless to say, as will be evident from examples presented in Section 2.4, incorporation of solid boundary effects complicates the mathematical structure of system (6).

2.3. Vortex Models as Control Systems

In this Section we recast system (7*a*)–(7*b*) modified to account for the presence of the solid boundaries and the free stream at infinity $\mathbf{u}_\infty$ as a generic control system. This will involve identifying explicitly the system *input* (control) and system *output* (measurements). Using this generic notation we will be able to analyze the investigations of vortex control problems carried out by different researchers in a uniform setting. Denoting the state vector of the system at time t $\mathbf{X}(t) \triangleq [x1(t)\ \ y1(t)\ \ \ldots\ \ x_N(t)\ \ y_N(t)]^T \in \mathbb{R}^{2N}$, the system evolution can be concisely expressed as (unless needed for clarity, we will skip the argument t)

$$\frac{d\mathbf{X}}{dt} = \mathbf{f}(\mathbf{X}), \tag{10}$$

where $\mathbf{f} : \mathbb{R}^{2N} \to \mathbb{R}^{2N}$ is the function describing the advection velocities of the vortices due to the induction of all the vortices and their images, as well as the effect of the free stream $\mathbf{u}_\infty$. Denoting $\mathbf{U} : \mathbb{R} \to \mathbb{R}^M$ a time–dependent control input with M degrees of freedom, autonomous system (10) can be generalized to include the actuation as follows

$$\frac{d\mathbf{X}}{dt} = \mathbf{f}(\mathbf{X}) + \mathbf{b}(\mathbf{X})\mathbf{U}, \tag{11a}$$

where $\mathbf{b}(\mathbf{X}) : \mathbb{R}^M \to \mathbb{R}^{2N}$ is the *control* operator describing how the actuation $\mathbf{U}$ affects the system dynamics. Evolution equation (11*a*) is complemented with an equation describing how the system output (measurements) $\mathbf{Y} \in \mathbb{R}^K$ is obtained, i.e.,

$$\mathbf{Y} = \mathbf{c}(\mathbf{X}) + \mathbf{D}\mathbf{U}, \tag{11b}$$

where $\mathbf{c} : \mathbb{R}^{2N} \to \mathbb{R}^K$ and $\mathbf{D} : \mathbb{R}^M \to \mathbb{R}^K$ are suitable observation operators. While the form of the function $\mathbf{f}$ is determined by (7*a*)–(7*b*) augmented, if necessary, to include the image

vortices and the free stream, the specific forms of the control operator **b** and the observation operators **c** and **D** will be made clear in the discussion of the different control problems in Sections 3 and 4. Denoting $\mathbf{X}_0$ an equilibrium solution of (10), i.e., a state such that $\mathbf{f}(\mathbf{X}_0) = \mathbf{0}$, $\mathbf{X}'(t) \triangleq [x'_1(t) \;\; y'_1(t) \;\; \ldots \;\; x'_N(t) \;\; y'_N(t)]^T \in \mathbb{R}^{2N}$ the vector of the perturbation variables and $\mathbf{Y}'$ the vector of the output perturbations, equations (11*a*) and (11*b*) can be linearized in a neighborhood of $\mathbf{X}_0$ yielding the *perturbation system*

$$\frac{d\mathbf{X}'}{dt} = \mathbf{A}\mathbf{X}' + \mathbf{B}\mathbf{U}, \tag{12a}$$

$$\mathbf{Y}' = \mathbf{C}\mathbf{X}' + \mathbf{D}\mathbf{U}, \tag{12b}$$

where $\mathbf{A} \triangleq \nabla\mathbf{f}(\mathbf{X}_0)$ and $\mathbf{C} \triangleq \nabla\mathbf{c}(\mathbf{X}_0)$ are the Jacobians of **f** and **c** evaluated at the equilibrium $\mathbf{X}_0$, whereas for the control operator we for simplicity assume here that $\mathbf{b}(\mathbf{X}) \equiv \mathbf{b}(\mathbf{X}_0)$, so that $\mathbf{B} = \mathbf{b}(\mathbf{X}_0)$. Approaches derived using the modern theory of optimal control make it possible to account systematically for the presence of modeling uncertainties and exogenous disturbances [7]. This is particularly relevant when control approaches derived based on point vortex models are then to be applied to problems governed by the Navier–Stokes system, including actual laboratory experiments. Modeling uncertainties are usually regarded as additive disturbances represented by a stochastic process w which is referred to as the *system (plant) noise*. It affects the linearized system dynamics (12*a*) via a $[2N \times 1]$ matrix **G** and the linearized system output (12*b*) via a $[K \times 1]$ matrix **H**. Furthermore, we assume that the system measurements may be additionally contaminated with noise $\mathbf{m} \triangleq [m_1 \;\; \ldots \;\; m_K]^T$, where $m_1, \ldots, m_K$ are also stochastic processes. With these definitions we can now put the linearized point vortex system into the standard state–space form which will serve as the basis for the development of methods based on the linear control theory [1, 7]

$$\frac{d\mathbf{X}'}{dt} = \mathbf{A}\mathbf{X}' + \mathbf{B}\mathbf{U} + \mathbf{G}w, \tag{13a}$$

$$\mathbf{Y}' = \mathbf{C}\mathbf{X}' + \mathbf{D}\mathbf{U} + \mathbf{H}w + \mathbf{m}. \tag{13b}$$

However, a majority of problems to be discussed below are in fact formulated in a purely deterministic setting, so that unless stated otherwise, we will assume that $w \equiv 0$ and $\mathbf{m} \equiv \mathbf{0}$. We finish this Section by stating two definitions of fundamental importance for the analysis of control system (13*a*)–(13*b*):

Definition 1 ([1, 7]) *System (13a) is said to be (state) controllable if, for any initial condition* $\mathbf{X}'(0)$*, it is always possible to determine a control* **U** *that will drive the system to an arbitrary final state* $\mathbf{X}'(T)$ *in a finite time* T*.*

Definition 2 ([1, 7]) *System (13a)–(13b) is said to be observable, if its state* $\mathbf{X}'$ *can always be reconstructed in finite time using only the system outputs* $\mathbf{Y}'$*.*

2.4. Vortex Equilibria in Flows Past Bodies

Evidently, important properties of perturbation system (13*a*)–(13*b*) will depend on the properties of the equilibrium $\mathbf{X}_0$ around which the linearization is performed. In problems involving flows past objects these vortex equilibria reveal some intriguing features which we

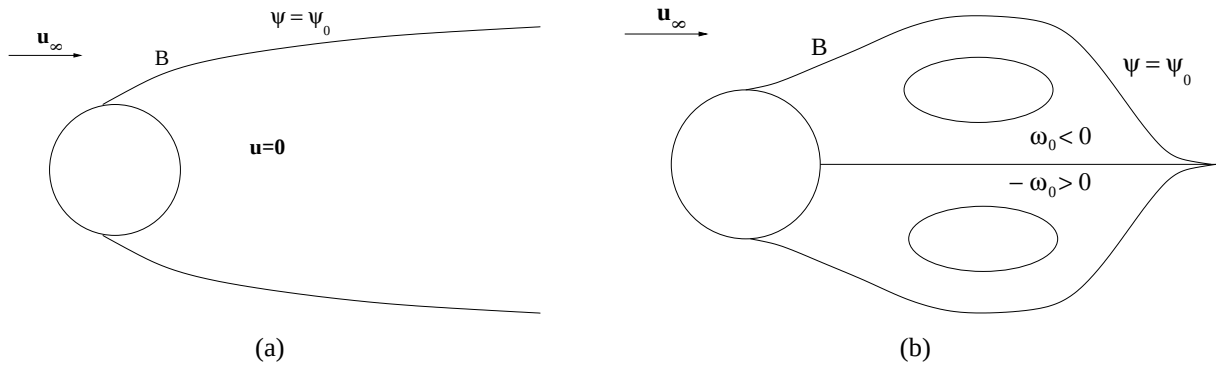

Figure 1. Schematic showing the main features of the recirculation zone in (a) Kirchhoff's model and (b) Batchelor's model of the steady wake flow in the infinite Reynolds number limit.

will now discuss starting with flows past bodies *without* a fixed separation point such as the circular cylinder. It is well–known that steady–state Euler equations (2) possess nonunique solutions, and that there is an infinite number of them. The question which of this infinite number of solutions is actually the *relevant* one, in the sense of being the infinite Reynolds number ($Re \to \infty$) limit of the corresponding solutions of the Navier–Stokes system, is one of fundamental questions of hydrodynamics which, as of yet, remain unanswered [55, 56]. Below we briefly present the main families of solutions that have been considered as possible candidates for this limit. Fundamentally, there are two such families: flows characterized by an *open* recirculation zone obtained using the "free–streamline" theory of Kirchhoff [57] (see Figure 1a), and flows featuring a *closed* recirculation zone arising as manifestations of the Prandtl–Batchelor theorem [40] (see Figure 1b).

In regard to the first class, the solutions are constructed by supposing the existence of a "free streamline" which separates the potential flow from a stagnation region behind the obstacle where the flow velocity vanishes identically [57, 30]. The pressure p_0 in the stagnation zone is assumed equal to the pressure at infinity p_∞, so that the free streamline coincides with a vortex sheet, with the jump B in the tangential velocity constant and equal to the free stream at infinity. For a given geometry the free–streamline model does not depend on any parameters. It can be shown [30] that Euler flows constructed in this way have a non–zero drag, and therefore do not give raise to d'Alembert's paradox.

Concerning the second class of flows, the Prandtl–Batchelor theorem [40] stipulates that in the infinite Reynolds number limit $Re \to \infty$ the regions in an incompressible flow characterized by closed streamlines must necessarily correspond to *constant* vorticity ω_0. In regard to Euler equation (2), this corresponds to the following choice of the RHS function $F(\psi)$

$$F(\psi) = -\omega_0 H(\psi_0 - \psi) - 2BH(\psi_0 - \psi), \tag{14}$$

where $H(\cdot)$ and $\delta(\cdot)$ are the Heaviside and Dirac distributions, which represents regions of constant vorticity $\omega_0 = \frac{\partial v}{\partial x} - \frac{\partial u}{\partial y}$ surrounded by a vortex sheet of strength B and embedded in an irrotational flow (the boundary of this vortex region is characterized by the condition $\psi = \psi_0$,

where $\psi_0 \in \mathbb{R}$ is a parameter). The strength B of the vortex sheet can also be interpreted as the jump of Bernoulli's constant when crossing the streamline $\psi = \psi_0$. Euler flows satisfying (2) with (14) and featuring a symmetric pair of counter–rotating vortices touching each other are referred to as "Sadovskii flows" [58] and were computed in unbounded domains by Pierrehumbert [59], and Saffman and Moore [60]. From the point of view of modeling bluff body wakes, the more relevant problem concerns finding Prandtl–Batchelor vortices in equilibrium with the cylinder. This problem was solved by Elcrat et al. [61] who also assumed for simplicity that $B = 0$, i.e., that there is no vortex sheet surrounding the vortex region. Elcrat et al. discovered several distinct families of such vortex flows, each depending on two parameters (Figure 2). The families consisting of vortex regions with *finite* area have the remarkable property that fixing the circulation $\Gamma = -\omega_0 \int_\Omega H(\psi_0 - \psi)\, d\Omega$ of an individual vortex patch and allowing its area to shrink to zero (i.e., $\psi_0 \to -\infty$) one obtains a continuous family of solutions approaching a point–vortex system in equilibrium with the obstacle as the asymptotic limit. In the case of the families characterized by pairs of vortex regions above / below the flow centerline and behind the obstacle, this point vortex solution is the one discovered by Föppl in 1913 [62]. The point vortex equilibrium corresponding to a pair of vortices behind the cylinder (Figure 2, top row, second column) is referred to as the "Föppl system". It has given rise to a number of interesting control problems, therefore below we provide a few details concerning this particular solution. The Föppl system consists of a pair of counter–rotating point vortices placed symmetrically above and below the flow centerline behind the cylinder (Figure 3a). These vortices are complemented by a pair of image vortices inside the cylinder whose location is determined by the circle theorem [30]. As shown already by Föppl, there exists a one–parameter family of Föppl systems characterized by the following algebraic relationship

$$\begin{cases} (|z_0|^2 - 1)^2 = 4|z_0|^2 y_0^2, \\ \Gamma = 2\pi \dfrac{(|z_0|^2 - 1)^2 (|z_0|^2 + 1)}{|z_0|^5}, \end{cases} \tag{15}$$

where $z_0 = x_0 + \mathrm{i}y_0$ is the position of the top vortex (the bottom vortex is located at $\overline{z}_0 = x_0 - \mathrm{i}y_0$), whereas $\Gamma = -\Gamma_1 = \Gamma_2$ is the circulation of the vortices. Thus, for every nonzero value of the circulation Γ there exists an equilibrium position of the vortices and this locus is referred to as the "Föppl line" (see also top row, first column in Figure 2). A remarkable property of Föppl equilibrium (15) is that its flow pattern features a recirculation bubble. In addition, the Föppl equilibrium possesses some interesting stability properties which will be reviewed in Section 2.5. As shown by Protas [63], one can generalize this "classical" Föppl system by incorporating in it higher–order terms representing the corrections due to the finite area of the vortex region, so that the new system can approximate with arbitrary accuracy the solutions of Euler equation (2) characterized by finite–area vortex regions, i.e., with the RHS given by (14). Below we outline the main idea of this construction. Consider a compact region P of vorticity embedded in an irrotational flow past a circular cylinder and characterized by a constant vorticity distribution ω_0. Using complex Green's function (4), the complex potential induced by such a vortex patch in a 2D unbounded domain can be expressed for points outside

the patch $z \notin P$ as

$$\tilde{W}_P(z) = (\varphi + \mathrm{i}\psi)(z) = \frac{\omega_0}{2\pi \mathrm{i}} \int_P \ln(z - z')\, dA(z'), \tag{16}$$

where $dA(z') = dx'dy'$. Tilde ($\tilde{}$) indicates that this potential represents a flow in a domain without boundaries, whereas the subscript indicates that the potential is due to the patch P. We now choose a point $z_s \in P$ as the origin of the local coordinate system associated with the patch P and set $\zeta = z' - z_s$. Complex potential (16) can now be expressed as

$$\tilde{W}_P(z) = \frac{\Gamma_0}{2\pi \mathrm{i}} \ln(z - z_s) + \frac{\omega_0}{2\pi i} \int_P \ln\left(1 - \frac{\zeta}{z - z_s}\right) dA(\zeta). \tag{17}$$

The second term in (17) can, for $|z - z_s| > |z' - z_s|$, be expanded in a Laurent series which yields

$$\tilde{W}_P(z) = \frac{\Gamma_0}{2\pi \mathrm{i}} \ln(z - z_s) - \frac{1}{2\pi \mathrm{i}} \sum_{n=1}^{\infty} \frac{c_n}{n} (z - z_s)^{-n}, \quad |z - z_s| > \zeta_m, \tag{18}$$

where

$$c_n(z_s) = \omega_0 \int_P \zeta^n\, dA(\zeta) \tag{19}$$

and $\zeta_m = \max_{(z_s+\zeta)\in P} |\zeta|$. Thus, the point z_s represents also the location of a singularity which, for the moment, remains unspecified. The quantities $c_n(z_s)$, $n = 1, \ldots, N_0$ are the moments of the vorticity distribution in the patch P with respect to the point z_s and therefore are related to the eccentricity of the patch (c_1), its ellipticity (c_2), etc. The zeroth moment c_0 is equal to the total circulation Γ_0 of the patch. The complex potential due to a finite–area vortex patch P can be approximated for points of the plane lying outside this patch by truncating expression (18), i.e., replacing it with a finite sum of singularities located at the point z_s

$$\tilde{W}_P(z) \cong \tilde{W}_{P,N_0}(z) = \frac{\Gamma_0}{2\pi \mathrm{i}} \ln(z - z_s) - \frac{1}{2\pi \mathrm{i}} \sum_{n=1}^{N_0} \frac{c_n}{n} (z - z_s)^{-n}, \quad |z - z_s| > \zeta_m. \tag{20}$$

The order of truncation N_0 is represented by the second subscript on $\tilde{W}$. The complex potential $\tilde{W}_{Q,N_0}(z)$ due to the patch Q with the opposite–sign vorticity $-\omega_0$ and located symmetrically below the flow centerline (Figure 1b) can be represented using an analogous expression in which z_s is replaced with $\overline{z}_s$ and c_n with $-\overline{c}_n$ for $n = 1, \ldots, N_0$. We now use these expressions to construct potential flows approximating solutions of the steady–state Euler equations in the sense that the velocity field of the potential flow will converge, for $z \notin P$ and $z \notin Q$, to the velocity field of the Euler flow as $N_0 \to \infty$. These potential flows are constructed using the potentials $\tilde{W}_{P,N_0}(z)$ and $\tilde{W}_{Q,N_0}(z)$, and employing the circle theorem [30] to generate suitable image singularities inside the obstacle in a way ensuring that the boundary conditions for the wall–normal velocity component are satisfied. As was shown in [63], the equilibrium

solutions of such "higher–order" Föppl systems are characterized by the condition

$$
\begin{aligned}
&U_\infty\left(1-\frac{R^2}{z_{N_0}^2}\right)-\frac{\Gamma_0}{2\pi\mathrm{i}}\left[-\frac{1}{\left(z_{N_0}-\frac{R^2}{\overline{z}_{N_0}}\right)}-\frac{1}{(z_{N_0}-\overline{z}_{N_0})}+\frac{1}{\left(z_{N_0}-\frac{R^2}{z_{N_0}}\right)}\right]\\
&+\frac{1}{2\pi\mathrm{i}}\sum_{n=1}^{N_0}\left[(-1)^{n+1}\frac{R^2\overline{c}_n}{\left(z_{N_0}-\frac{R^2}{\overline{z}_{N_0}}\right)^{n+1}}\frac{z_{N_0}^{n-1}}{\overline{z}_{N_0}^{n+1}}\right.\\
&\left.-\frac{\overline{c}_n}{(z_{N_0}-\overline{z}_{N_0})^{n+1}}-(-1)^{n+1}\frac{R^2c_n}{\left(z_{N_0}-\frac{R^2}{z_{N_0}}\right)^{n+1}}\frac{1}{z_{N_0}^2}\right]=0
\end{aligned}
\tag{21}
$$

which is a complex–valued equation characterizing one complex unknown z_{N_0}, i.e., the N_0–order Föppl equilibrium. The sum in Equation (21) represents the N_0–order correction to the classical Föppl system resulting from the finite area of the vortex region. Assuming a fixed circulation Γ_0 of this vortex region, the higher–order Föppl equilibria z_{N_0} represent a two–parameter family of solutions of (21) depending on the truncation order N_0, which is a discrete parameter, and the set of moments $c_n(z_0)$, $n=1,\ldots,N_0$, which vary continuously with the area $|A|$ of the vortex region desingularizing classical Föppl equilibrium (15). Thus, when $N_0=0$ we recover the classical Föppl system with one equilibrium given by (15). In the case $N_0\geq 1$ the qualitative and quantitative properties of the loci of the higher–order equilibria z_{N_0} were studied in [63]. While a detailed review of these results is beyond the scope of the present paper, we mention one result which is quite relevant to the vortex control problem. In [63] it was proven that, for a fixed truncation order N_0, the locus of equilibrium solutions z_{N_0} forms a curve parametrized by the area $|A|$ of the vortex region and starting at the classical equilibrium z_0. Therefore, the higher–order equilibria z_{N_0} can be regarded as perturbations of the classical equilibrium z_0 such that the distance $|z_{N_0}-z_0|$ is a continuous function of the area $|A|$ of the vortex region desingularizing classical equilibrium (15) (Figure 3b). We conclude this discussion by remarking that all the flows belonging to the Prandtl–Batchelor family of solutions of (2), together with the limiting point–vortex systems, are characterized by *zero* drag.

The question of existence of vortex equilibria becomes more subtle when one considers flows past objects with fixed separation points, such as corners or cusps. In such cases the flow must satisfy one additional condition, namely the Kutta–Joukowski condition, which requires that the separation should occur at a singular point. In the context of equation (2) this is enforced by specifying the value of the streamfunction at a point adjacent to the prescribed separation point, thereby restricting the class of possible solutions. Indeed, the flow past a finite plate normal to the oncoming uniform stream [64] is an example of a potential flow in which no vortex equilibrium exists that would also satisfy the Kutta–Joukowski condition (in fact, in the past some authors had staked claims to the opposite effect, and we refer the reader to [26] for some interesting remarks concerning the history of this problem). This issue was recently revisited by Zannetti [65] who investigated the existence of point vortices in equilibrium with a flow past a locally deformed wall that also need to satisfy the

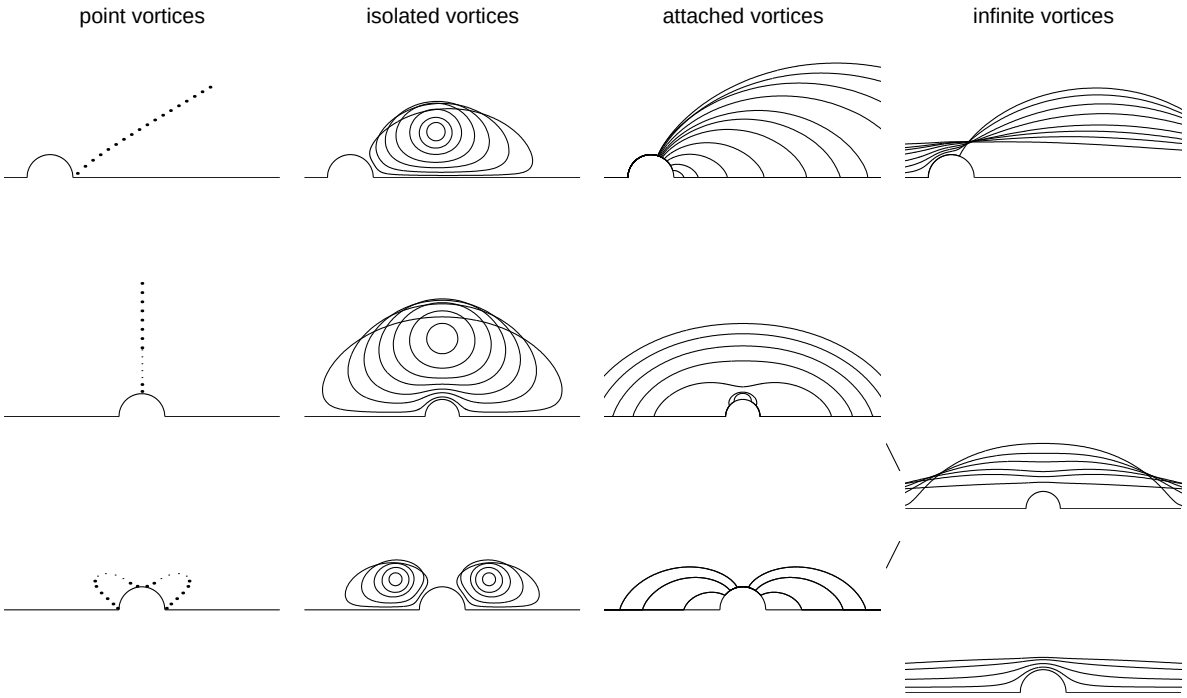

Figure 2. (first column) One–parameter families of point vortices in equilibrium with the cylinder and (remaining columns) the associated two-parameter families of isolated, attached and infinite vortex regions computed in [61]. The family of infinite vortices (fourth column) is a perturbation of the potential flow. [Figure reproduced with permission of the publisher (Cambridge University Press).]

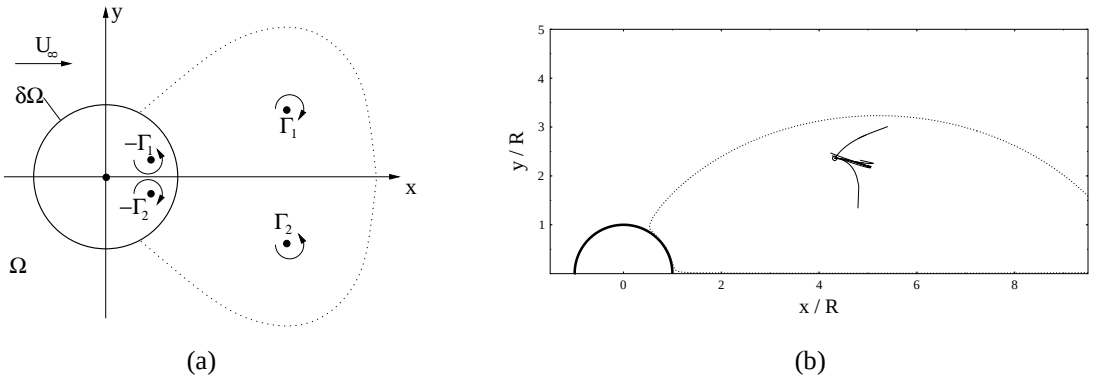

(a) (b)

Figure 3. (a) Schematic of the classical Föppl system; the dashed line represents the separatrix streamline delimiting the recirculation bubble, (b) loci of the higher–order Föppl equilibria z_{N_0} parametrized by the area $|A|$ of the vortex region for different truncation orders ($N_0 = 1,3,5,10,15$) [63]; the circle represents the classical Föppl equilibrium.

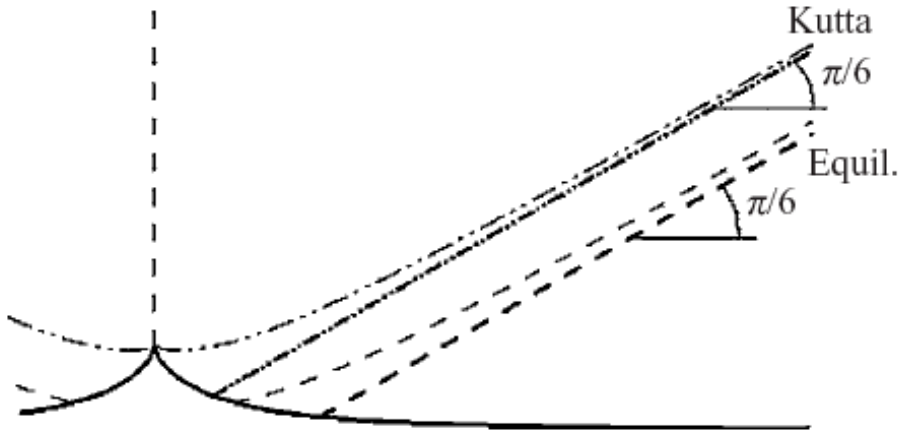

Figure 4. The Föppl ("Equil.") and Kutta manifolds with their asymptotes showing no intersection points [65]; the domain boundary is in the form of a symmetric Ringleb snow cornice [46]. [Figure reproduced with permission of the publisher (Cambridge University Press).]

Kutta–Joukowski condition. The problem was analyzed by studying the intersection points of the "Föppl manifold", representing the locus of the point vortex equilibria, and the "Kutta manifold" representing the locus of point vortices satisfying the Kutta–Joukowski condition. Criteria concerning the existence of such intersection points were linked to the geometry of the domain, more specifically, to the properties of the conformal mapping employed to transform the original domain into the half–plane. In particular, it was shown that there exist domain boundaries with fore–and–aft symmetry for which the Föppl and Kutta manifolds do not intersect, so that there is no vortex equilibrium satisfying the Kutta–Joukowski condition (Figure 4).

The same questions also pertain to the problem of existence of finite–area vortex regions described by equations (2) and (14), and also required to satisfy the Kutta–Joukowski condition. In this regard it was conjectured by Zannetti in [65] that nonexistence of a *point vortex* in equilibrium with the flow and satisfying at the same time the Kutta–Joukowski condition would preclude the existence of the corresponding family of finite–area vortex regions satisfying analogous conditions. While this issue is currently under investigation, claims supporting an opposite point of view had been made by Turfus et al. [66, 67]. The latter results however were recently questioned by Gallizio [68] as a computational artifact related to insufficient numerical resolution. On the other hand, when the body placed in the flow does not possess the fore–and–aft symmetry, it is possible to find equilibrium point vortex configurations satisfying the Kutta–Joukowski condition. Indeed, using an inclined flat plate as the obstacle, Saffman and Sheffield [45] found several families of equilibrium vortex configurations satisfying the Kutta–Joukowski condition, and one such solution is shown in Figure 5a. Such solutions are in fact quite interesting from the practical point of view, because configurations as shown in Figure 5a feature an increased lift as compared to the flow without

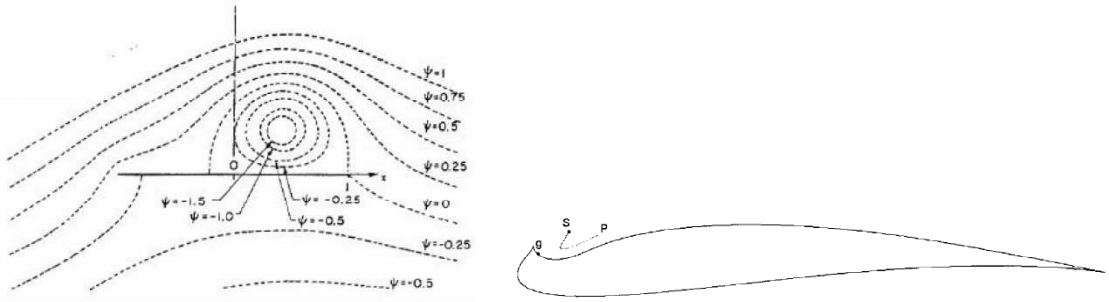

(a) (b)

Figure 5. (a) Streamline pattern in one of the equilibrium solutions found by Saffman and Sheffield [45] and involving a vortex attached to an inclined flat plate; (b) modified Joukowski airfoil with a cornice–shaped cavity ("Kasper wing"); equilibrium position of the vortex in the cavity is denoted *S* [121]. [Figures reproduced with kind permission of the publishers (Wiley-Blackwell and Springer Science for Figures (a) and (b), respectively).]

attached vortices. Since most such equilibrium solutions are linearly unstable, one possibility to obtain more robust configurations consists in "trapping" the vortices in a suitably–designed cavity on the upper surface of the airfoil (Figure 5b). The shape of the cavity is closely related to a "snow cornice" and one of the first investigators to study vortex equilibria in such geometries was Ringleb [46]. The concept of a vortex trapped in a cornice–shaped cavity on the top surface of an airfoil, known also as the "Kasper wing" [69], has been explored in the aerospace industry [70] and still remains the subject of intense research efforts [71]. The existence of solutions characterized by finite regions of constant vorticity, i.e., satisfying (2) with (14) in addition to the Kutta–Joukowski condition, in such geometries was stipulated by Bunyakin et al. [72], however, to the author's best knowledge, such flows have not actually been computed yet. There also exist other models of the wake flows corresponding to the $Re \to \infty$ limit, such as the Riabouchinsky flow [73] which is a hybrid unifying some features of the Kirchhoff and Prandtl–Batchelor flows. However, we will not discuss them here, since they do not strictly satisfy Euler equations (2).

A salient feature of real flows past bluff bodies is the spontaneous formation of an array of counter–rotating vortices, the so–called Bénard–von Kármán vortex street, when the Reynolds number is sufficiently high. This phenomenon was first modeled mathematically using point vortices by von Kármán [74] who found equilibrium configurations of two arrays of point vortices extending indefinitely in the upstream and downstream directions. Von Kármán also established that, while the symmetric arrangements are always unstable, the staggered arrangements are linearly stable, but only for certain combinations of the intra–vortex separations and the distance between the two lines of vortices, a result that was subsequently made more precise by Heisenberg [75]. This class of models was also studied by Villat [76] and was recently revisited using modern techniques by Aref et al. [77] who found more complicated equilibrium patters involving several arrays of vortices. A weakness shared by all models based on periodic arrangements of vortices is that they extend to infinity also in the upstream direction, so that it is not possible to account for the presence of the solid

body generating the wake. This is most likely the reason why such vortex models have not been investigated in the context of flow control problems.

2.5. Stability of Vortex Equilibria in Flows Past Bodies

Having surveyed different vortex configurations in equilibrium with solid bodies, we now turn to an analysis of their stability. These properties are going to play a central role in the development of methods based on the optimal control theory. We will focus on analyzing the stability of the Föppl system, since this is the equilibrium configuration whose stability has been researched the most thoroughly. As will be argued later, many other vortex equilibria have analogous properties as regards the linear stability. The stability properties of the classical Föppl system and their relevance for the modeling of transition to vortex shedding were thoroughly analyzed by Tang & Aubry [78]. In an earlier study, Smith [79] identified an error in Föppl's original derivation which concerned the stability of solution (15) with respect to symmetric perturbations. This issue was again revisited by Cai et al. [80] who also derived a more general stability criterion and applied it to study the stability of point vortices in equilibrium with elliptic cylinders and circular cylinders with splitter plates. De Laat & Coene [81] analyzed the frequency of the neutrally stable oscillatory mode as a function of the downstream coordinate x_0. The linear stability analysis of the Föppl system is performed by adding the perturbations $z_1' \triangleq x_1' + \mathrm{i}y_1'$ and $z_2' \triangleq x_2' + \mathrm{i}y_2'$ to the coordinates $z_1 = x_0 + \mathrm{i}y_0$ and $z_2 = x_0 - \mathrm{i}y_0$ of the upper and lower vortex in equilibrium solution (15), and then linearizing governing system (10) around $\mathbf{X}_0 = [x_0 \;\; y_0 \;\; x_0 \;\; -y_0]^T$ assuming small perturbations (Figure 6a). Thus, evolution of the perturbations is governed by system (12*a*) where $\mathbf{X}' = [x_1' \;\; y_1' \;\; x_2' \;\; y_2']^T$ and $\mathbf{B} \equiv \mathbf{0}$, and the system matrix $\mathbf{A}$ is given by (see [78])

$$\mathbf{A} = \begin{bmatrix} a & b & c & d \\ e & -a & f & c \\ c & -d & a & -b \\ -f & c & -e & -a \end{bmatrix} \tag{22}$$

with the following entries

$$\begin{aligned} a &= \frac{3x_0}{|z_0|^6} - \frac{2x_0}{|z_0|^8}, \\ b &= \frac{1}{|z_0|^9} - \frac{5}{2|z_0|^7} + \frac{1}{2|z_0|^5} + \frac{2}{|z_0|^3} + \frac{1}{|z_0|}, \\ c &= -\frac{x_0}{|z_0|^4}, \\ d &= -\frac{1}{2|z_0|^5} - \frac{1}{2|z_0|^3} - \frac{1}{|z_0|}, \\ e &= \frac{1}{|z_0|^9} - \frac{5}{2|z_0|^7} - \frac{3}{2|z_0|^5} + \frac{1}{|z_0|}, \\ f &= \frac{1}{2|z_0|^5} - \frac{3}{2|z_0|^3} - \frac{1}{|z_0|}. \end{aligned} \tag{23}$$

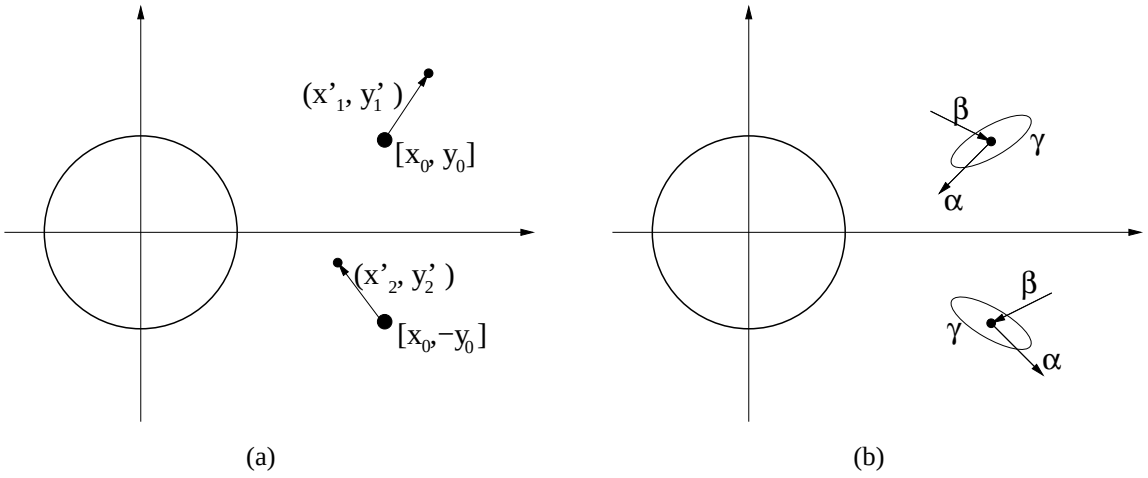

Figure 6. (a) Schematic indicating the perturbations $\mathbf{X}'$ of the classical Föppl equilibrium $\mathbf{X}_0$; the big dots represent the equilibrium and the small dots represent the perturbed positions, (b) the three modes of motion characterizing the linearized Föppl system with the system matrix **A** given in (22); note that another pair of the modes α and β can be obtained by reversing the direction of the corresponding eigenvectors.

We remark that (12*a*) is a linear time–invariant (LTI) system. Eigenvalue analysis of the matrix **A** reveals the presence of the following modes of motion (Figure 6b):

- unstable (growing) mode α corresponding to a positive real eigenvalue $\lambda_1 = \lambda_r > 0$,
- stable (decaying) mode β corresponding to a negative real eigenvalue $\lambda_2 = -\lambda_r < 0$,
- neutrally stable oscillatory mode γ corresponding to a conjugate pair of purely imaginary eigenvalues $\lambda_{3/4} = \pm i\lambda_i$.

These qualitative properties are independent of the downstream coordinate x_0 parameterizing equilibrium solution (15). The linearized system is neutrally stable to symmetric perturbations and unstable to almost all asymmetric perturbations. Furthermore, analysis of the orientation of the unstable eigenvectors of **A** carried out in [78] revealed that the initial stages of instability of the Föppl system closely resemble the onset of the vortex shedding in an actual cylinder wake undergoing the Hopf bifurcation. A question naturally arising in this context concerns the stability of the solutions of Euler equation (2) with (14) which desingularize the classical Föppl solution, cf. Figure 2. This problem was investigated in [82] where it was shown that, in analogy with the classical Föppl system discussed above, the Jacobians of such solutions are characterized by one unstable and one exponentially stable mode in addition to an infinite number of neutrally stable modes. The nonlinear stability of Föppl equilibrium (15) has received only limited attention: it was studied in a weakly nonlinear setting by Tordella [83] and recently for a more general system using the energy–Casimir methods by Shashikanth et al. [84].

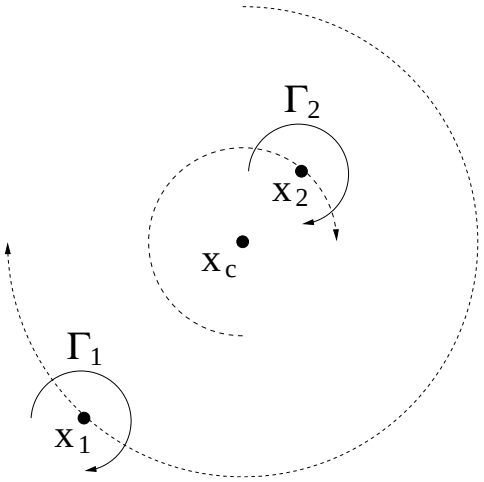

Figure 7. Schematic of a co–rotating vortex pair; dotted lines represent vortex trajectories.

3. Control of Vortex Flows in Domains without Boundaries

As compared to the results concerning vortex flows in domains with boundaries, which will be reviewed in Section 4, the results concerning optimal control of vortex flows in domains without boundaries are relatively few. The reason appears to be that such configurations represent a fairly idealized setting not connected directly to any specific application. In this context we mention the work of Vainchtein and Mezić [85], elaborated further in [86], who considered the problem of optimal control of a co–rotating vortex pair. Such a system of two same–sign vortices represents the simplest point vortex system with nontrivial behavior (Figure 7). The nominal dynamics consists of the two vortices moving in opposite directions on circular trajectories around their vorticity centroid $\mathbf{x}_c \triangleq \frac{\Gamma_1\mathbf{x}_1+\Gamma_2\mathbf{x}_2}{\Gamma_1+\Gamma_2}$. The control objective in that investigation was twofold, namely, to move $\mathbf{x}_c$ from an initial to a desired location and to change the vortex separation $2r \triangleq \|\mathbf{x}_1-\mathbf{x}_2\|$ from some initial to a desired value using (i) a uniform strain field and (ii) a field due to a localized source or sink as the actuation. The authors considered "adiabatic" control where it was assumed that the control field was a small (of order ε) perturbation of the nominal velocity field. This made it possible to apply the method of averaging [87] which "averaged out" the fast rotation of the vortices around $\mathbf{x}_c$ yielding in this way a reduced system for the averaged quantities $\langle\mathbf{x}_c\rangle$ and $\langle r\rangle$ as the new state variables. For example, in the case of the uniform strain field used as the control, governing equation (11a) for the control system now takes the specific form

$$\frac{d\langle\mathbf{x}_c\rangle}{dt} = \mathbf{b}(\langle\mathbf{x}_c\rangle)\mathbf{U}, \tag{24}$$

where $\mathbf{b}(\langle\mathbf{x}_c\rangle) = [\langle x_c\rangle \quad -\langle y_c\rangle]^T$. The solutions of this averaged system describe the behavior of the original state variables with an accuracy $O(\varepsilon)$ over time intervals $O(\varepsilon^{-1})$ [87]. In the case when the strain field was used as the control, the optimal protocols could be found applying direct methods of calculus to minimize the cost of the control. Assuming the control input to be bounded in the mean sense over a cycle of vortex rotation resulted

in an impulsive control in the form of a combination of Dirac delta measures applied at optimal phases of the vortex rotation. On the other hand, assuming the control input to be bounded at all times resulted in a "bang–bang" control in which the actuation either vanishes, or is equal to its maximum allowed value. The "bang–bang" control often arises in optimal control problems in which the control is restricted by some lower and upper bound, and the resulting solution for the optimal control intermittently switches between these two values [7]. In the case when a sink / source was employed as the actuation, the solution of the optimal control problem was more complicated and required the use of the Pontryagin maximum principle applied to the averaged equations. The Pontryagin maximum principle is a general technique providing necessary conditions characterizing the solution of optimal control problems involving constraints on both the state and the control [7]. This approach will be described in more detail in the context of another control problem in Section 4.2; here we mention only that it also resulted in an optimal control in the form of a set of Dirac delta measures applied at the optimal phases of the vortex rotation. A generalization of this problem was considered by the same authors in [23] where the point vortices were replaced with elliptic vortex patches possessing more internal degrees of freedom. A solution of the associated problem of state estimation for a co–rotating vortex pair was proposed by Tadmor [88] and will be discussed in Section 5.

4. Control of Vortex Flows in Domains with Boundaries

Control of vortex flows in domains with boundaries has attracted significant attention. This in particular concerns vortex flows past objects such as plates, bluff bodies and airfoils placed in a uniform stream which serve as models of flows arising in many important applications. In order to place the following discussion in an appropriate context, we begin by stating some general results concerning control and stabilization of 2D Euler equation (2) in a domain with boundaries. The following result is due to Coron [89]:

Theorem 1 *If the controls act on an arbitrary small open subset* Σ *of the boundary* $\partial\Omega$ *which meets every connected component of this boundary, then 2D Euler equation (2) is exactly controllable.*

The proof of this theorem relies on the so–called "return method" and for further details concerning this proof we refer the reader to the monograph [89] which also outlines the relevant control–theoretic background. Theorem 1 has the physically–relevant implication that, if the control does not act on certain internal boundary segments of a multiply–connected domain, then the Euler system in that domain may not be controllable, which is a consequence of the fact that such control will not have the authority over some cyclic motions (i.e., motions with prescribed circulations around holes in the domain).

4.1. Control of Vortex Flows in Bounded Domains

One of the first systematic studies of a vortex control problem in a domain with boundaries was the investigation by Péntek, Kadtke and Toroczkai [90] who employed methods of "chaos

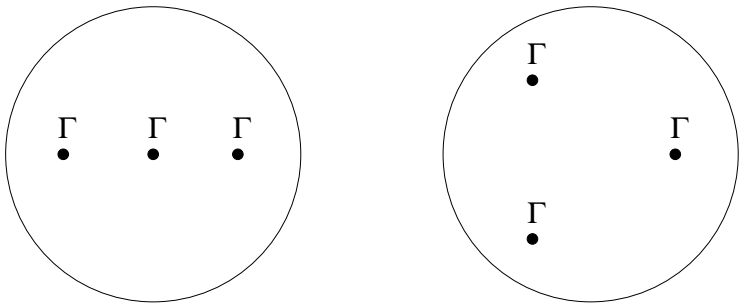

Figure 8. (a,b) Symmetric three–vortex configurations with unstable periodic orbits whose stabilization was investigated in [90] using the OGY approach; each configuration rotates with a specific angular velocity (figures not to scale).

control" [91] allowing one to stabilize an otherwise unstable periodic orbit embedded in the chaotic attractor of the system. Péntek et al. studied the problem of controlling symmetric arrays of three same–sign point vortices contained in a closed circular container (Figure 8). As is well known, such simple systems already exhibit nonintegrable (chaotic) behavior in addition to the presence of unstable periodic motion related to the rotation of the vortex array as a rigid body. In terms of the actuation, the authors used mass transpiration distributed on the cylinder boundary and characterized by three degrees of freedom. Control was performed using an OGY feedback algorithm due to Ott, Grebogi and Yorke [92]. The idea of this method is to adjust the actuation at every discrete instant of time so as to drive the state of the system towards the *stable* manifold of the fixed point one seeks to stabilize. In this way only a small control input is required, as most of the work is done by the internal dynamics (i.e., the transfer along the stable manifold). The OGY approach requires that an eigenvector ξ_s of the Jacobian $\mathbf{A}$ associated with the stable manifold of the equilibrium $\mathbf{X}_0$ be available. Then, the OGY control method relies on the following ansatz

$$\mathbf{X}'(t+\Delta t) = a\|\mathbf{X}'(t)\|\xi_s, \tag{25}$$

where $\Delta t \ll 1$ is the time step and $a \in (0.1)$ is a real parameter. Relation (25) should be regarded as a condition on the control input $\mathbf{U}$ which requires it to align the perturbation $\mathbf{X}'$ at the following time level with the stable subspace of the Jacobian $\mathbf{A}$, so that the natural dynamics of the system can bring it to the unstable equilibrium $\mathbf{X}_0$. Using (12a) to re–express (25) we obtain

$$\frac{1}{\Delta t}\left[a\|\mathbf{X}'(t)\|\xi_s - (\mathbf{I}+\Delta t\mathbf{A})\mathbf{X}'(t)\right] = \Delta t\mathbf{B}\mathbf{U} + O(\Delta t^2). \tag{26}$$

Truncating the terms proportional to Δt^2, one obtains a system of linear equations that need to be solved in order to obtain the control $\mathbf{U}(t)$ at the present instant of time. Evidently, when $M < 2N$, system (26) may not have any solutions. This difficulty was circumvented by the authors in [90] by requiring that the perturbation $\mathbf{X}'$ reach the stable manifold after p steps, i.e., replacing (25) with a modified ansatz

$$\mathbf{X}'(t+p\Delta t) = a\|\mathbf{X}'(t)\|\xi_s, \tag{27}$$

so that (26) would now become

$$\frac{1}{\Delta t}\left[a\|\mathbf{X}'(t)\|\xi_s-(\mathbf{I}+\Delta t\mathbf{A})^p\mathbf{X}'(t)\right]= \\ =(\mathbf{I}+\Delta t\mathbf{A})^{p-1}\mathbf{B}\mathbf{U}(t)+(\mathbf{I}+\Delta t\mathbf{A})^{p-2}\mathbf{B}\mathbf{U}(t+\Delta t)+\ldots+\mathbf{B}\mathbf{U}(t+p\Delta t)+O(\Delta t^2). \tag{28}$$

which can be solved for $\{\mathbf{U}(t),\mathbf{U}(t+\Delta t),\ldots,\mathbf{U}(t+p\Delta t)\}$ provided p is chosen so that $pM\geq 2N$ [for $pM>2N$, system (28) is underdetermined and some values of the control input can be set equal to zero]. Remarkably, the study [90] also was the first investigation which employed methods of the modern control theory to study the controllability of the vortex systems shown in Figure 8a,b which allowed the authors to identify the forms of actuation with insufficient control authority (e.g., changing the shape of the domain boundary from cylindrical to elliptical). We postpone a detailed discussion of the controllability concept to Section 4. The computational results reported in [90] confirmed that the OGY control strategy was indeed capable of preventing the chaotic behavior by maintaining the periodic motion. The OGY approach was also applied to control vortex systems in unbounded domains which will be reviewed in Section 4.

The next investigation we discuss in this category is the optimal control of a point vortex in a potential "corner flow" studied by Noack et al. in [93] (Figure 9a). The objective in this control problem was to enhance mixing which was quantified by considering a time–averaged integral of the mass flux across an invariant manifold of the Poincaré map characterizing particles' trajectories. This invariant manifold is a union of the stable and unstable manifolds emanating from the stable and unstable fixed points of the Poincaré map (Figure 9b). In Figure 9b we can also see the regions occupied by the fluid entrained and detrained to and from the recirculation zone, denoted D and E, respectively. The state variable was the position of the vortex $\mathbf{X}=[x_v\ \ y_v]^T$ and the control actuation had the form of a perturbation of the potential stream in the corner flow and was characterized by one time–dependent parameter, so that in (11*a*) we have $\mathbf{U}\in\mathbb{R}$ and

$$\mathbf{b}(\mathbf{X})=k\begin{bmatrix}x_v\\-y_v\end{bmatrix}, \tag{29}$$

where $k\in\mathbb{R}$ is a parameter . A key result demonstrated in [93] was that the above control problem can be solved by transforming governing equation (11*a*) with $\mathbf{b}(\mathbf{X})$ given by (29) to the *flat coordinates* $z_1=\alpha_1(x_v,y_v)$ and $z_2=\alpha_2(x_v,y_v)$, where α_1 and α_2 are suitably chosen transformations. With thus redefined state variables, the governing system takes the form

$$\frac{d}{dt}\begin{bmatrix}z_1\\z_2\end{bmatrix}=\begin{bmatrix}z_2\\p(z_1,z_2)\end{bmatrix}+\begin{bmatrix}0\\q(z_1,z_2)\end{bmatrix}\mathbf{U}. \tag{30}$$

We note that the first new dependent variable (the flat coordinate) z_1 can be prescribed as $z_1=z_1^d$, where z_1^d is some chosen function, and the corresponding control can be determined afterward as

$$\mathbf{U}=\frac{\dot{z}_2^d-p(z_1^d,z_2^d)}{q(z_1^d,z_2^d)} \tag{31}$$

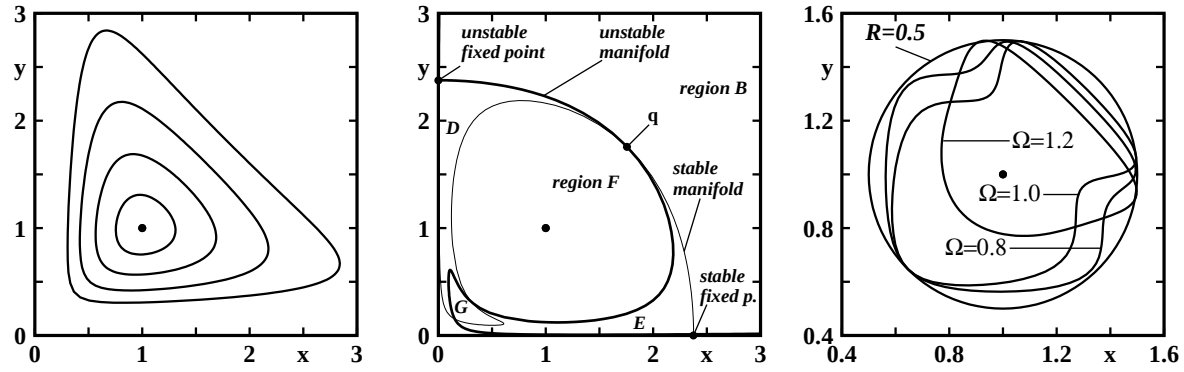

Figure 9. Corner flow with a point vortex studied in [93]: (a) the uncontrolled system with the solid symbol denoting the equilibrium position and the lines representing periodic orbits, (b) features of the Poincaré map of particle trajectories corresponding to the natural vortex dynamics, and (c) optimal vortex trajectories with the corresponding frequencies of rotation. [Reprinted with permission from [93]. Copyright (2004), American Institute of Physics.]

provided $q \neq 0$ and $z_2^d = \dot{z}_1^d$. Thus, existence of an invertible transformation to the flat coordinates is equivalent to controllability of the original system. The trajectory z_1^d was then represented with a few Fourier basis functions whose coefficients were optimized computationally using a linear programming (simplex) algorithm to maximize the cost functional, and examples of optimal vortex trajectories from [93] are shown in Figure 9c. Noack et al. presented also a general theory concerning transformation of equations of vortex motion (11a) to the flat coordinates in arbitrary domains and in situations involving multiple vortices. The flux–maximizing optimal control $\mathbf{U}^{opt}$ is clearly of an "open–loop" type, and it is not evident if the corresponding optimal trajectory would in practice be stable with respect to disturbances and modeling errors. Therefore, Noack et al. proposed to stabilize control law (31) with proportional feedback terms, so that it would now take the form

$$\mathbf{U} = \frac{\dot{z}_2^d - p(z_1, z_2) - k_1(z_1 - z_1^d) - k_2(z_2 - z_2^d)}{q(z_1, z_2)}, \tag{32}$$

where the coefficients k_1 and k_2 were chosen to ensure that the deviations $z_1 - z_1^d$ and $z_2 - z_2^d$ vanish with time. For such feedback stabilization to be applicable in practical settings one must be able to recover the instantaneous values of z_1 and z_2 from some measurements of the systems. In [93] this was accomplished employing a suitably–designed observer whose discussion is however deferred to Section 7. For completeness we also mention investigations [94] and [95] which employed 2D vortex models to study the effect of various passive flow control strategies in engineering applications.

4.2. Control of Vortex Flows Past Bodies

We now proceed to discuss investigations concerning control of different vortex flows in domains with internal boundaries. Some of the first systematic studies of this problem were

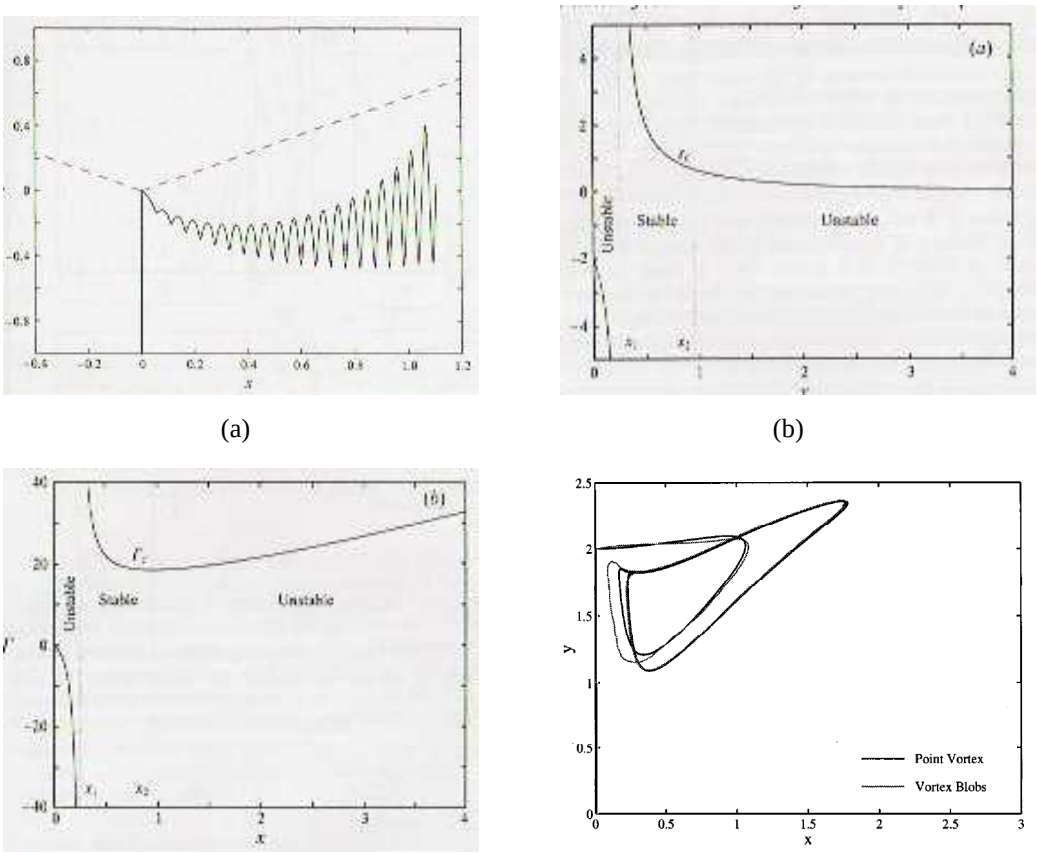

Figure 10. (a) Trajectory of the vortex under the action of the nonlinear feedback controller developed in [96] to ensure invariance of the vortex circulation; the dashed lines divide the flow domain into different controllability regions, the values of (b) the steady actuation **U** and (c) circulation Γ corresponding to the equilibrium solutions of the controlled system discussed in [97]; note that the positive circulation corresponds to the clockwise rotating vortices, a convention which is opposite to the one adopted everywhere else in this paper, (d) trajectories of a single vortex and the vorticity centroid (i.e., the collective coordinate) of the high–order model proposed in [98]. [Figures (a), (b) and (c) reproduced with permission of the publisher (Cambridge University Press). Figure (d) reprinted with permission from [98]. Copyright (1997), American Institute of Physics.]

carried out by Cortelezzi et al. [96, 97, 98]. The first study [96] was concerned with the control of the unsteady separated flow past a semi–infinite plate with the transverse motion of the plate serving as the actuation (Figure 10a). The roll–up of the separated shear layer was modeled by a point vortex whose time–dependent circulation was predicted using an unsteady Kutta condition. When circulations of the point vortices are allowed to change during the flow evolution, equations governing the particle trajectories [cf. (7*a*)–(7*b*)] need to be modified, for instance, by incorporating the so–called Brown–Michael correction [99]. Using the condition that the circulation of the vortex remain constant, a nonlinear feedback control algorithm was designed in [96] that determines the instantaneous transverse velocity of the plate as a function

of the instantaneous coordinates of the vortex. Using methods of nonlinear dynamical systems it was then shown that the state space of the system, coinciding with the flow domain, consists of three controllability regions separated by rays emanating from the separation point along which controllability was lost (Figure 10a). In this Figure we also notice that, despite the fact that the vortex circulation remains constant, the vortex is swept downstream and exhibits oscillations with the amplitude increasing with the downstream distance. This effect was accompanied by a systematic increase of the magnitude of the actuation. The following investigation [97] concerned a similar flow configuration, except that the plate was assumed to be finite, the vortices were assumed to separate symmetrically from the top and bottom edges, whereas the flow actuation had the form of a blowing / suction point modeled as a source / sink at the rear side of the plate. As in the earlier investigation, a nonlinear controller was found which ensures the circulation of the shed vortices stays constant. This is equivalent to containing the wake to a pair of counter–rotating vortices that remain attached to the obstacle. Furthermore, it was also shown in [97] that the steady–state actuation corresponding to a forced equilibrium solution of the point vortex system can be found in an explicit form (the expressions are rather lengthy and therefore we do not quote them here). As is evident from Figure 10b,c, the forced equilibrium exhibits an interesting behavior characterized by a bifurcation of the actuation value: for vortices with anti–clockwise circulation the required actuation is in the form of blowing and the resulting equilibrium locus is close to the plate; on the other hand, for vortices with clockwise circulation the required actuation is in the form of suction and the resulting equilibrium locus extends downstream. For vanishing actuation the flow configuration becomes symmetric with respect to the Y–axis and, in agreement with Zannetti's criteria [65] discussed in Section 2.4, does not admit equilibrium solutions. Only a limited section of the equilibrium locus was shown to be linearly stable, and the associated basin of attraction represents the vortex configurations that can be stabilized with this approach. Numerical simulations performed for a flow with a periodically oscillating free stream velocity indicated that the system approached a limit cycle with the vortex on a closed trajectory circumscribing the equilibrium position corresponding to a steady free stream. A similar behavior will later be shown to occur also in other controlled vortex systems. An interesting extension of this control approach was proposed in [98] where the authors studied the possibility of transferring a control strategy determined for a simpler ("lower–order") model to a more complex ("higher–order") model. This is in fact a very relevant problem, because given the complexity of the mathematical techniques involved, a rigorous design of the controller is often possible only for significantly simplified models, whereas accurate description of the system usually requires that more complete models be used. In terms of the higher–order model, the authors proposed in [98] a vortex "blob" system which, comparing to the model introduced in [97], consisted of a larger number of particles, each of which was characterized by a finite core size (i.e., a desingularized point vortex). A "bridge" linking the lower–order and higher–order models is the *collective coordinate* which determines the state of the lower–order model corresponding to the state of the higher–order model, thereby making it possible to apply to the latter a control law derived for the former. For vortex systems such a collective coordinate can be the position of a vortex that represents a "cloud"

of vortex blobs used in the higher–order model. The locus of such a substitute point vortex can be determined by enforcing the conservation of the total circulation and the linear momentum which in the presence of solid boundaries is a somewhat delicate matter, as it requires one to also take into account the image vortices. Numerical computations employing this approach and reported in [98] confirmed that the structure of the equilibrium loci in the lower-order model and the higher–order model (expressed in terms of the collective coordinates) are qualitatively equivalent. Likewise, the behavior of the controlled system in the presence of free–stream fluctuations was quite similar in both cases and featured vortex trajectories approaching a limit cycle (Figure 10d).

The nonlinear controllers investigated in [96, 97, 98] provide closed–form expressions for the actuation, but require *complete* information about the state of the system and the mathematical model which in practical situations may be difficult to obtain. An approach which relaxes these requirements was studied in [100] where the problem of controlling the higher–order model from [98] was considered. The goal was to design a "black–box" controller that will not require any information about the mathematical model of the system, and will only use the system *output* in the form of some measurements, for instance of the velocity at some point at the rear side of the plate, so that the observation operator $\mathbf{c}$ in (12*b*) is given by

$$\mathbf{c}(\mathbf{X}) = [-\Im[V(z_m)]] - \mathbf{DU}, \tag{33}$$

where $z_m \triangleq x_m + \mathrm{i}y_m$ is a measurement point located downstream of the plate, whereas $\mathbf{D} = \Im\left[\frac{z_m+1}{z_m(z_m-1)}\right]$ represents the velocity induced at the measurement point by the source / sink and is included in (33) in order to remove the feed–through effect. A generic framework for such feedback control is provided by the Proportional–Integral–Differential (PID) controller [7]. In [100] the authors employed a simplified version of this approach, namely, the Proportional–Integral (PI) controller in which the instantaneous actuation $\mathbf{U}(t)$ was assumed proportional to a measure of the instantaneous error $\varepsilon(t)$ between the actual output $\mathbf{Y}(t)$ [cf. (12*b*) with (33)] and the prescribed output $\tilde{\mathbf{Y}}(t)$, and also proportional to the error accumulated over some time window and represented by an integral of $\varepsilon(t)$, Thus, denoting t_k the current time step and setting $\varepsilon(t) = \|\mathbf{Y}(t) - \tilde{\mathbf{Y}}(t)\|$, the discrete PI control algorithm yields

$$\begin{aligned}\mathbf{U}(t_k) &= -K_P\varepsilon(t_k) - K_I\sum_{l=1}^{k}\frac{\varepsilon(t_l)+\varepsilon(t_{l-1})}{2}\Delta t \\ &= \mathbf{U}(t_{k-1}) - \left(K_P + K_I\frac{\Delta t}{2}\right)\varepsilon(t_k) - \left(-K_P + K_I\frac{\Delta t}{2}\right)\varepsilon(t_{k-1}),\end{aligned} \tag{34}$$

where K_P and K_I are proportionality constants and the trapezoidal rule was used to approximate the integral. We emphasize that the simple PID / PD approach does not guarantee optimality of the control in any sense. With a steady free stream at infinity, the PD approach performed similarly to the controller derived by Cortelezzi et al. in [98], i.e., it was able to stabilize the system and contain the wake to a pair of counter–rotating vortices attached to the obstacle (analogous performance was also obtained when the total circulation, or the circulation centroid was used as the system output). However, when the free stream was allowed to oscillate, the resulting state of the system and the system output exhibited

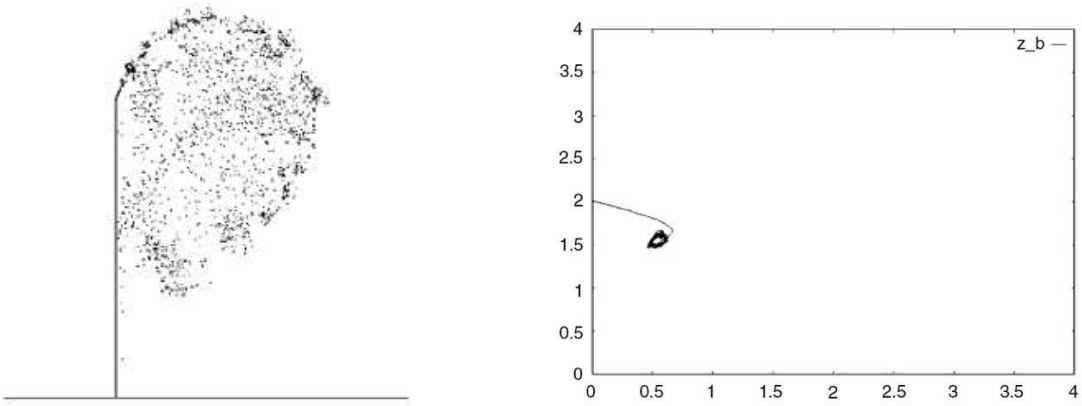

(a) (b)

Figure 11. (a) Instantaneous positions of vortex blobs and (b) the corresponding time–dependent trajectory of the center of circulation in the flow past a flat plate broadside to the oncoming stream with a steady suction applied at the real wall [101]. [Figures reproduced from [101] with kind permission of the publisher (Springer Science and Business Media).]

significant oscillations, an effect not observed when the nonlinear controller of [98] was applied. As a step towards resolving this problem, the authors developed in [100] a system identification (SI) strategy. In an effort to keep the present Section focused, we defer the discussion of this strategy to Section 5.

The problem of controlling vortices interacting with a flat plate was also addressed by Zannetti and Iollo [101] who considered the more general configuration of the plate at an arbitrary angle with respect to the oncoming flow. The principal finding of this investigation was that a forced vortex equilibrium can in fact be established applying *steady* suction at the rear side of the plate, i.e., no feedback is necessary. The authors also argued that applying such steady actuation has a similar effect to replacing a straight plate with a cambered one, in the sense that the resulting breaking of the symmetry with respect to the Y–axis makes it possible for the equilibrium solutions to also satisfy the Kutta conditions at the separation point (cf. the discussion of the relationship between the symmetry of the domain and the existence of intersection points of the Föppl and Kutta manifolds in Section 2.4). The results of the mathematical analysis were illustrated applying the steady actuation to a time–dependent vortex–blob model of the wake past a plate oriented broadside to the oncoming flow, i.e., a problem analogous to the higher–order model studied in [98]. The computations confirmed the feasibility of this approach and in Figure 11 we reproduce a sample result concerning the evolution of the vortex blobs (Figure 11a) and the corresponding trajectory of the center of circulation in the controlled flow, i.e., the collective coordinate (Figure 11b). We remark that this center of circulation approaches a circular trajectory circumscribing the equilibrium position of the point vortex system, a generic behavior already observed in Figure 10b.

Several investigations addressed the problem of controlling chaotic trajectories of point vortices advected by the free stream and interacting with a circular cylinder in uniform rotation. While a single point vortex in such a configuration follows a regular trajectory

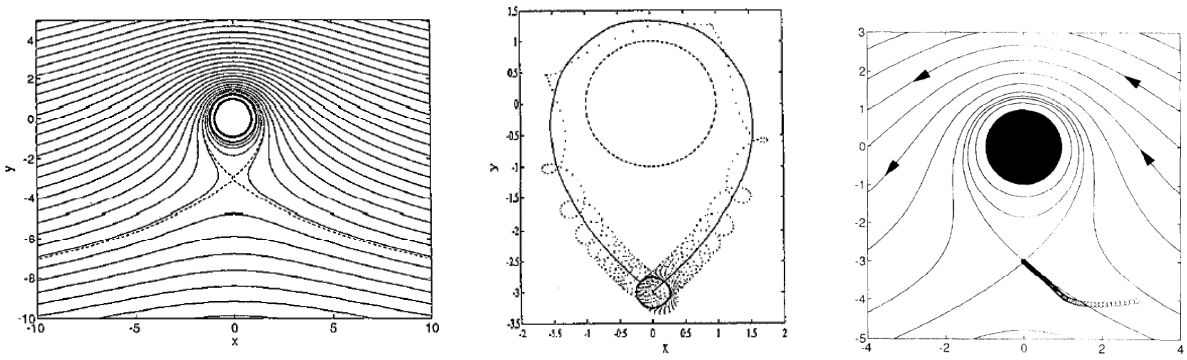

(a) (b) (c)

Figure 12. (a) Streamlines of a system consisting of a single vortex interacting with a cylinder considered in [102]; the intersection point of the dotted line represents the unstable equilibrium of this system, (b) trajectory of the center of vorticity of a chaotic vortex pair in an analogous configuration as in (a); the dotted line represents the trajectory of one of the vortices [102], (c) convergence of the point vortices (denoted by empty circles) to the unstable equilibrium under the action of the OGY control scheme [103] (note that the flow in Figures (a)–(c) is from the right to the left). [Figures (a) and (b) reprinted with permission from [102]. Copyright (1994), American Institute of Physics. Figure (c) reproduced from [103] with permission of the publisher (Elsevier).]

(Figure 12a), when the system integrability is destroyed by imposing a time–dependent perturbation to the free stream [102], or replacing the point vortex with a vortex pair [103], the trajectories of the vortex (pair) become chaotic. A signature of this chaotic behavior are the "capture events" during which the time of interaction between the vortex (pair) and the cylinder is significantly longer then otherwise (Figure 12b). The unperturbed system has an unstable equilibrium (a saddle) located directly below the cylinder (for the free stream approaching from the right and the cylinder rotating in the counterclockwise direction). The problem of stabilizing this equilibrium was studied by Chernyshenko in [104] who used a zero mass flux transpiration, modeled as a point source–sink pair, as the actuation. Employing methods of asymptotic analysis similar to the averaging technique investigated by Vainchtein and Mezić [86] (see Section 3), it was demonstrated that a high–frequency alternating blowing and suction can modify the type of stability of this equilibrium from a saddle to a center, thereby rendering the equilibrium neutrally stable. Another method to stabilize this equilibrium, based on the OGY approach [92], was proposed by Kadtke, Péntek and Pedrizzetti [103] who applied the cylinder rotation as the actuation. A result indicating the success of this approach is reproduced in Figure 12c. The OGY control approach derived in [103] based on a simple point vortex system was then applied in a similar setting to control the flow of a viscous fluid described by the Navier–Stokes equation, and the computations reported in [105] showed a good performance of this control method.

Next we go on to discuss investigations concerning the control of the classical Föppl system described in Section 2.4. In our opinion, out of all the vortex dynamics problems, this configuration has received the most complete characterization from the control–theoretic

point of view. The first control study concerning this problem was the work of Tang and Aubry [106] who considered a *passive* technique based on including in system (10) a symmetric pair of counter–rotating control vortices with the circulations $\pm\Gamma_c$ and *fixed* locations $z_c = x_c + \mathrm{i}y_c$ and $\bar{z}_c = x_c - \mathrm{i}y_c$ (Figure 13a). Thus, the actuation function $\mathbf{b}(\mathbf{X})\mathbf{U}$ in (11a) was given by

$$\mathbf{b}(\mathbf{X})\mathbf{U} = \mathbf{b}(\mathbf{X}) = \frac{\Gamma_c}{2\pi}\begin{bmatrix} \Re\left(\frac{\mathrm{i}}{z_1-z_c}+\frac{\mathrm{i}}{z_1-\bar{z}_c}+\frac{\mathrm{i}}{z_1-1/\bar{z}_c}-\frac{\mathrm{i}}{z_1-1/z_c}\right) \\ -\Im\left(\frac{\mathrm{i}}{z_1-z_c}+\frac{\mathrm{i}}{z_1-\bar{z}_c}+\frac{\mathrm{i}}{z_1-1/\bar{z}_c}-\frac{\mathrm{i}}{z_1-1/z_c}\right) \\ \Re\left(\frac{\mathrm{i}}{z_2-z_c}+\frac{\mathrm{i}}{z_2-\bar{z}_c}+\frac{\mathrm{i}}{z_2-1/\bar{z}_c}-\frac{\mathrm{i}}{z_2-1/z_c}\right) \\ -\Im\left(\frac{\mathrm{i}}{z_2-z_c}+\frac{\mathrm{i}}{z_2-\bar{z}_c}+\frac{\mathrm{i}}{z_2-1/\bar{z}_c}-\frac{\mathrm{i}}{z_2-1/z_c}\right) \end{bmatrix}. \tag{35}$$

Interestingly, the classical Föppl system augmented with actuation (35) was shown to possess, for sufficiently large values of Γ_c, two new families of solutions (Figure 14). Remarkably, one of these new families was shown to be neutrally stable with the Jacobian $\mathbf{A} = \nabla\mathbf{f}(\mathbf{X}_0) + \nabla\mathbf{b}(\mathbf{X}_0)$ characterized by purely imaginary eigenvalues only. Thus, by introducing in the flow a suitably chosen pair of control vortices, the original *linearly unstable* configuration (cf. Section 2.5) could be replaced with a modified *neutrally stable* configuration, a behavior that, as was demonstrated in [106] using numerical computations, also occurs for the viscous fluid flow governed by the 2D Navier–Stokes equation. However, a disadvantage of this control strategy from the practical point of view is the difficulty of introducing and maintaining control vortices with fixed circulations and locations.

The next investigation concerning the control of the Föppl system, carried out by Li and Aubry [107], employed a slow and small–amplitude transverse motion of the cylinder described by the vertical displacement $\delta(t)$ as the flow actuation (Figure 13b). The goal was to construct a *feedback* control algorithm that would instantaneously adjust this actuation in order to cancel the lift force at every instant of time. As is well known [109], the lift force is intrinsically related to *asymmetry* of the vorticity distribution in the wake, and therefore can be considered a signature of a developing symmetry–breaking instability. In the context of the controlled point vortex model (11a) the cylinder displacement was represented as a vortex sheet with the strength $\Gamma_e(t,\gamma)$, where γ is the azimuthal angle (Figure 13b), appearing on the cylinder boundary in response to the perturbation of the velocity boundary condition resulting from the displacement $\delta(t)$ (cf. our discussion of the different methods for enforcing boundary conditions in potential flows in Section 2.2). Noting that, in the first–order approximation, $\Gamma_e(t,\gamma) = -2\cos(\gamma)\frac{\partial\delta(t,\gamma)}{\partial t}$, the actuation term in (11a) takes the form [107]

$$\mathbf{b}(\mathbf{X})\mathbf{U} = \frac{1}{2\pi}\begin{bmatrix} \Re\left(2\mathrm{i}\int_0^{2\pi}\frac{\cos(\gamma)}{z_1-z_\delta}d\gamma\right) \\ -\Im\left(2\mathrm{i}\int_0^{2\pi}\frac{\cos(\gamma)}{z_1-z_\delta}d\gamma\right) \\ \Re\left(2\mathrm{i}\int_0^{2\pi}\frac{\cos(\gamma)}{z_2-z_\delta}d\gamma\right) \\ -\Im\left(2\mathrm{i}\int_0^{2\pi}\frac{\cos(\gamma)}{z_2-z_\delta}d\gamma\right) \end{bmatrix}\frac{\partial}{\partial t}\delta(t,\gamma), \tag{36}$$

where $z_\delta(\gamma) \triangleq \mathrm{e}^{\mathrm{i}\gamma} + \mathrm{i}\delta(t)$ is a point on the boundary of the displaced cylinder. The control input $\delta(t)$ was determined by the condition that the lift be equal to zero at every instant of

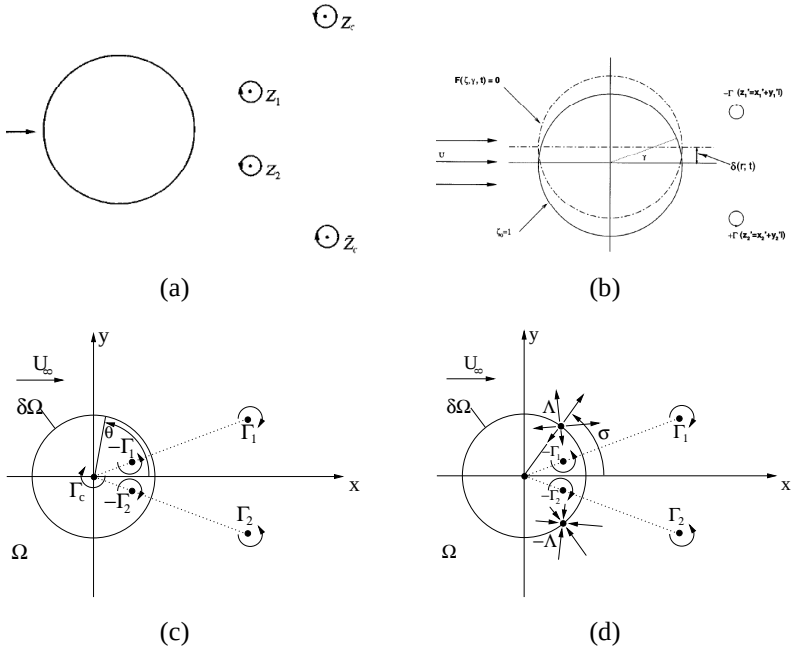

Figure 13. Different forms of actuation considered in the stabilization studies of the Föppl system: (a) control vortices at z_c and $\overline{z}_c$ introduced in [106], (b) transverse motion of the cylinder studied in [107], (c) cylinder rotation represented by a vortex Γ_C inside the contour and (d) blowing and suction modeled by a source–sink pair with intensity Λ investigated in [108]. [Figures (a) and (b) reprinted with permission from [106] and [107], respectively. Copyright (2000,2003), American Institute of Physics.]

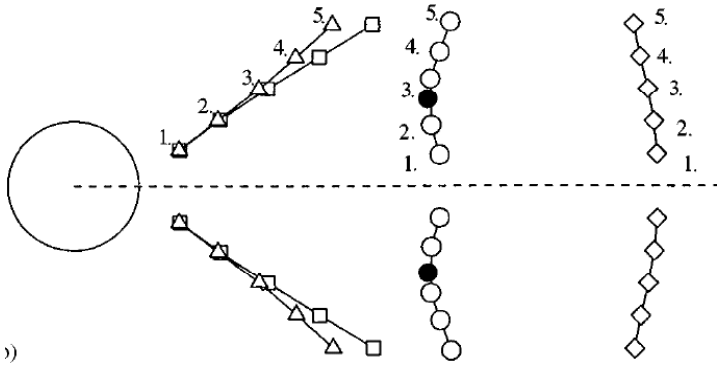

Figure 14. (Squares) The equilibrium locus of uncontrolled system (15) (the "Föppl line") and (triangles, circles, and diamonds) the three equilibrium loci obtained in the Föppl system using the passive control developed in [106] with the circulation of the control vortices equal to $\Gamma_c = 0.06\pi$ and the locations $z_c = 5.392 + 1.35\mathrm{i}$, $\overline{z}_c = 5.392 - 1.35\mathrm{i}$. The circulations Γ of the Föppl vortices are as indicated [106]. [Figure reproduced with permission of the publisher (Elsevier).]

time which, after using asymptotic expansions in (36) and retaining the leading–order (linear) terms only, resulted in the following closed–form expression for the displacement

$$\delta(t) = a(\mathbf{X}_0)\rho_A(t) + b(\mathbf{X}_0)\alpha_A(t), \tag{37}$$

where $a(\mathbf{X}_0)$ and $b(\mathbf{X}_0)$ are functions determined by the equilibrium state $\mathbf{X}_0$ and available in closed forms, whereas $\rho_A(t) \triangleq \sqrt{(x_1')^2 + (y_1')^2} - \sqrt{(x_2')^2 + (y_2')^2}$ and $\alpha_A(t) \triangleq \arctan(y_1'/x_1') - \arctan(y_2'/x_2')$. We emphasize that the form of feedback relation (37) is such that the displacement $\delta(t)$ depends on the *asymmetric* part only of the perturbation from equilibrium (15) and described by the quantities $\rho_A(t)$ and $\alpha_A(t)$. While investigation [107] did not furnish any a priori control–theoretic guarantees concerning the performance of this controller, the computational results concerning its application to a 2D viscous wake flow governed by the Navier–Stokes equation indicated that it was essentially able to eliminate the lift force in that case as well.

Control problems for the Föppl system were investigated using methods of the modern control theory by the present author [108, 110, 111]. The goal of this research effort has been to design optimal output–feedback control algorithms to stabilize system (12*a*) and at the same time extremize some measure of performance represented by a suitable cost functional. In terms of the actuation, these investigations primarily focused on using the cylinder rotation represented by a point vortex with the circulation $\mathbf{U} = \Gamma_C(t)$ located inside the cylinder (Figure 13c). We remark that a vortex system with such an actuation does not in fact satisfy Kelvin's principle [30, 31] which stipulates that in an inviscid flow the circulation along any material contour is conserved (when a time–dependent actuation $\Gamma_C(t)$ is applied, the circulation along the cylinder boundary is equal to $\Gamma_C(t)$ and hence is not constant). Since Kelvin's principle is applicable to *inviscid* flows only, deviations from this principle may be regarded as a way of accounting qualitatively for viscous effects (after all, actuating a real flow via cylinder rotation is essentially a viscous effect). This admittedly simple form of actuation was also employed in [103]. Another form of actuation considered briefly in [108] used wall transpiration distributed over the cylinder boundary and modeled as a source–sink pair (Figure 13d). The source–sink pair was assumed to have a zero net flux, hence at every instant of time t it is fully determined by a single parameter $\mathbf{U} = \Lambda(t)$. As shown in [108], the control matrices corresponding to the two forms of actuation are given by (Figure 13c,d)

$$\mathbf{B}_\Gamma \triangleq \frac{1}{2\pi|z_0|^2}\begin{bmatrix} -y_0 \\ x_0 \\ y_0 \\ x_0 \end{bmatrix}, \tag{38}$$

$$\mathbf{B}_\Lambda \triangleq -\frac{\sin(\sigma)}{\pi(\chi^2+\kappa^2)}\begin{bmatrix} \kappa \\ \chi \\ \kappa \\ \chi \end{bmatrix}, \tag{39}$$

where $\chi \triangleq x_0^2 - y_0^2 - 2x_0\cos(\sigma) + 1$ and $\kappa \triangleq -2y_0[x_0 - \cos(\sigma)]$. In order to formulate an optimal control problem we need to identify a cost functional that the control algorithm will

seek to minimize. This cost functional will be expressed in terms of system outputs, i.e., certain measurable quantities that characterize the system evolution [cf. (13*b*)], and the system input, i.e., the control $\mathbf{U}$. Investigation [108] focused on attenuation of vortex shedding as the control objective which was quantified by measuring the velocity at a point $z_m = x_m + \mathrm{i}0$ on the flow centerline. Choosing this quantity as the system output, equation (11*b*) becomes

$$\mathbf{Y} \triangleq \begin{bmatrix} \Re[V(x_m)] \\ -\Im[V(x_m)] \end{bmatrix} + \mathbf{D}\Gamma_C, \tag{40}$$

where the matrix $\mathbf{D} \triangleq \frac{1}{2\pi x_m^2}[0 \quad x_m]^T$ represents the feed–through effect of the control on the measurements (i.e., the control–to–measurements map). This particular choice of the observation operator $\mathbf{c}(\mathbf{X})$ was motivated by practical considerations, as pointwise velocity measurements are relatively easy to implement in a laboratory experiment (for instance, using a hot wire). Linearizing relation (40) around the Föppl equilibrium $\mathbf{X}_0$ we obtain (12*b*) in which the linearized observation operator is given by

$$\mathbf{C}_v = \begin{bmatrix} \left.\frac{\partial u(x_m)}{\partial x_1}\right|_{(x_0,y_0)} & \left.\frac{\partial u(x_m)}{\partial y_1}\right|_{(x_0,y_0)} & \left.\frac{\partial u(x_m)}{\partial x_2}\right|_{(x_0,y_0)} & \left.\frac{\partial u(x_m)}{\partial y_2}\right|_{(x_0,y_0)} \\ \left.\frac{\partial v(x_m)}{\partial x_1}\right|_{(x_0,y_0)} & \left.\frac{\partial v(x_m)}{\partial y_1}\right|_{(x_0,y_0)} & \left.\frac{\partial v(x_m)}{\partial x_2}\right|_{(x_0,y_0)} & \left.\frac{\partial v(x_m)}{\partial y_2}\right|_{(x_0,y_0)} \end{bmatrix}, \tag{41}$$

where $u(x_m) + \mathrm{i}v(x_m) = V(x_m)$. In investigation [108] we also considered other possible forms of the system output, such as the pressure difference $\Delta p(\varphi) \triangleq p(\varphi) - p(-\varphi)$ between two points located symmetrically above and below the flow centerline and making with it an angle φ and $-\varphi$, respectively. The quantity $\Delta p(\varphi)$ is important, since $-\int_0^\pi \Delta p(\varphi)\sin(\varphi)\,d\varphi$ represents the form lift. In a potential flow with known velocity field the pressure at a given boundary point can be calculated from the Bernoulli equation as $p_\varphi = p_0 + \frac{1}{2}(|V_0|^2 - |V_\varphi|^2)$, where p_0 and V_0 are the pressure and the complex velocity at some arbitrary point belonging to the streamline which coincides with the boundary, and V_φ is the complex velocity at the boundary point. Thus, the vertical pressure difference can be expressed as $\Delta p = \frac{1}{2}(|V_{-\varphi}|^2 - |V_\varphi|^2)$ and the corresponding linearized observation operator is [cf. (12*b*)]

$$\mathbf{C}_{\Delta p} = \left[\left.\frac{\partial \Delta p(\varphi)}{\partial x_1}\right|_{(x_0,y_0)} \quad \left.\frac{\partial \Delta p(\varphi)}{\partial y_1}\right|_{(x_0,y_0)} \quad \left.\frac{\partial \Delta p(\varphi)}{\partial x_2}\right|_{(x_0,y_0)} \quad \left.\frac{\partial \Delta p(\varphi)}{\partial y_2}\right|_{(x_0,y_0)} \right]. \tag{42}$$

Our objective is to find a *feedback* control law $\mathbf{U} = -\mathbf{K}\mathbf{X}'$, where $\mathbf{K}$ is a $[1 \times 4]$ feedback matrix, that will stabilize system (13*a*) while minimizing a performance criterion represented by the following cost functional

$$\mathcal{J}(\mathbf{U}) \triangleq E\left[\int_0^\infty (\mathbf{Y}'^T\mathbf{Q}\mathbf{Y}' + \mathbf{U}^T\mathbf{R}\mathbf{U})dt\right], \tag{43}$$

where E denotes the expectation, $\mathbf{Q}$ is a symmetric positive semi–definite matrix and $\mathbf{R}$ is a symmetric positive–definite matrix. Cost functional (43) is defined in a statistical sense (i.e., using an expectation), because governing system (13*a*)–(13*b*) may include stochastic disturbances. We remark that cost functional (43) balances the linearized system output $\mathbf{Y}'$ [i.e., the linearized velocity at the sensor location $(x_m, 0)$, or the linearized pressure difference on the cylinder boundary] and the control effort, whereas the feedback control law provides a recipe for determining the actuation (i.e., the circulation of the control vortex Γ_C representing

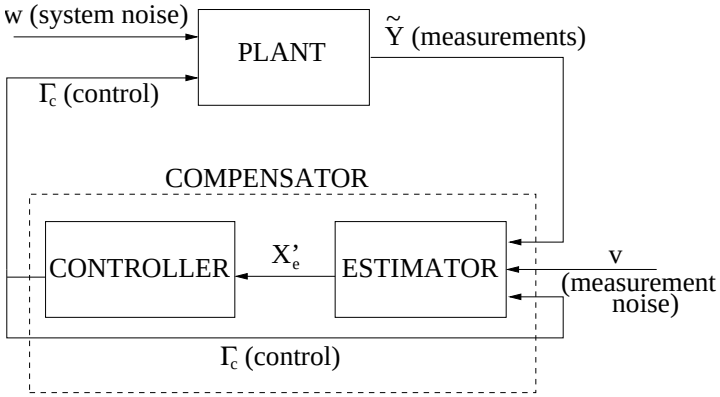

Figure 15. Schematic of a compensator composed of an estimator and a controller.

the cylinder rotation, or the intensity Λ of the mass transpiration) based on the state of the linearized system (i.e., the perturbation $\mathbf{X}'$ of the equilibrium $\mathbf{X}_0$). In practice, however, the state $\mathbf{X}'$ will not be known. Instead, some noisy and possibly incomplete measurements $\tilde{\mathbf{Y}} \in \mathbb{R}^K$ of the actual system [i.e., nonlinear Föppl model (11*a*) or another plant that the control strategy is applied to] are available and can be used in an *estimation procedure* to construct a time–dependent estimate $\mathbf{X}'_e$ of the model state $\mathbf{X}'$. The evolution of the state estimate $\mathbf{X}'_e$ is governed by the *estimator* system [1, 7]

$$\frac{d}{dt}\mathbf{X}'_e = \mathbf{A}\mathbf{X}'_e + \mathbf{B}\mathbf{U} + \mathbf{L}(\tilde{\mathbf{Y}} - \mathbf{Y}_e), \tag{44a}$$

$$\mathbf{Y}_e \quad = \mathbf{C}\mathbf{X}'_e + \mathbf{D}\mathbf{U}, \tag{44b}$$

where $\mathbf{L}$ is a feedback matrix that can be chosen in a manner ensuring that the expectation of the estimation error vanishes in the infinite time horizon, i.e., that $E[\|\mathbf{X}'_e - \mathbf{X}'\|] \to 0$ as $t \to \infty$. Thus, the estimator assimilates available observations into the system model, so as to produce an evolving estimate of the state of the system. Finally, the controller and the estimator can be combined to form a *compensator* in which the feedback control is determined based on the state estimate $\mathbf{X}'_e$ as

$$\mathbf{U} = -\mathbf{K}\mathbf{X}'_e, \tag{45}$$

rather than the actual state $\mathbf{X}'$. The flow of information in a compensator is shown schematically in Figure 15. The compensation problem can thus be stated as follows:

Problem 5 (compensation) *Assuming that the disturbances w and* $\mathbf{m}$ *in (13a) and (13b) are white, zero–mean and Gaussian, determine the feedback gains* $\mathbf{K}$ *and* $\mathbf{L}$ *for the controller and estimator systems (13a)–(13b) with (45) and (44a)–(44b), respectively, that will minimize cost functional (43) in addition to stabilizing the controller and estimator systems.*

Before we set out to design a compensator for system (13*a*)–(13*b*), we need to analyze the control system in order to verify that this is in fact feasible given the internal structure of the Föppl system with its different possible inputs and outputs. This can be done by investigating controllability and observability of system (13*a*)–(13*b*).

For a linear time–invariant system such as (12*a*) it is possible to assess controllability by examining a simple algebraic condition for the matrix pair $\{\mathbf{A},\mathbf{B}\}$, and in [108] it was shown that

$$N_\Gamma \triangleq \text{rank}\left[\mathbf{B}_\Gamma \;\; \mathbf{A}\mathbf{B}_\Gamma \;\; \mathbf{A}^2\mathbf{B}_\Gamma \;\; \mathbf{A}^3\mathbf{B}_\Gamma\right] = 2, \tag{46}$$

$$N_\Lambda \triangleq \text{rank}\left[\mathbf{B}_\Lambda \;\; \mathbf{A}\mathbf{B}_\Lambda \;\; \mathbf{A}^2\mathbf{B}_\Lambda \;\; \mathbf{A}^3\mathbf{B}_\Lambda\right] = 4. \tag{47}$$

Since $N_\Gamma < N = 4$, linearized Föppl system (12*a*) with the cylinder rotation ($\mathbf{B}_\Gamma$) used as the actuation is *not* controllable. On the other hand, since $N_\Lambda = N = 4$, when the blowing and suction ($\mathbf{B}_\Lambda$) is used as the actuation, linearized system (13*a*) is fully controllable.

By the same token, it is possible to assess observability of system (12*a*)–(12*b*) by examining a simple algebraic condition for the matrix pair $\{\mathbf{A},\mathbf{C}\}$, and in [108] it was shown that

$$N_v \;\; \triangleq \text{rank}\left[\mathbf{C}_v^T \;\; \mathbf{A}^T\mathbf{C}_v^T \;\; (\mathbf{A}^T)^2\mathbf{C}_v^T \;\; (\mathbf{A}^T)^3\mathbf{C}_v^T\right] = 4, \tag{48}$$

$$N_{\Delta p} \triangleq \text{rank}\left[\mathbf{C}_{\Delta p}^T \;\; \mathbf{A}^T\mathbf{C}_{\Delta p}^T \;\; (\mathbf{A}^T)^2\mathbf{C}_{\Delta p}^T \;\; (\mathbf{A}^T)^3\mathbf{C}_{\Delta p}^T\right] = 2. \tag{49}$$

Thus, since $N_v = N = 4$, linearized system (12*a*)–(12*b*) with the centerline velocity measurements ($\mathbf{C}_v$) is observable. On the other hand, when the pressure difference on the cylinder boundary Δp is used as the system output ($\mathbf{C}_{\Delta p}$), the linearized Föppl system is not observable. Hereafter we will focus on the case when the cylinder rotation is used as the control (i.e., $\mathbf{U} = \Gamma_C$ and $\mathbf{B} = \mathbf{B}_\Gamma$) and the centerline velocity measurements are used as the system output (i.e., $\mathbf{C} = \mathbf{C}_v$). We note that the difference $N - N_\Gamma = 2$ is equal to the number of modes which are not controllable [7], and it is illuminating to see which modes cannot actually be controlled. For this purpose we can deduce a *minimal representation* of system (13*a*)–(13*b*) consisting of those modes only which are both controllable and observable. This can be done by introducing an orthogonal transformation matrix

$$\mathbf{T}_c \triangleq \sqrt{2}\begin{bmatrix} 1/2 & 0 & -1/2 & 0 \\ 0 & 1/2 & 0 & 1/2 \\ 1/2 & 0 & 1/2 & 0 \\ 0 & 1/2 & 0 & -1/2 \end{bmatrix} \tag{50}$$

and making the following change of variables $\mathbf{X}'_{ab} \triangleq \begin{bmatrix} \mathbf{X}'_a \\ \mathbf{X}'_b \end{bmatrix} = \mathbf{T}_c\mathbf{X}'$. The corresponding form of system (13*a*)–(13*b*) is

$$\frac{d}{dt}\begin{bmatrix} \mathbf{X}'_a \\ \mathbf{X}'_b \end{bmatrix} = \begin{bmatrix} \mathbf{A}_a & \mathbf{0} \\ \mathbf{0} & \mathbf{A}_b \end{bmatrix}\begin{bmatrix} \mathbf{X}'_a \\ \mathbf{X}'_b \end{bmatrix} + \begin{bmatrix} \mathbf{B}_a \\ \mathbf{0} \end{bmatrix}\Gamma_C + \begin{bmatrix} \mathbf{G}_a \\ \mathbf{G}_b \end{bmatrix} w, \tag{51a}$$

$$\begin{bmatrix} Y_b \\ Y_a \end{bmatrix} = \begin{bmatrix} \mathbf{0} & \mathbf{C}_b \\ \mathbf{C}_a & \mathbf{0} \end{bmatrix}\begin{bmatrix} \mathbf{X}'_a \\ \mathbf{X}'_b \end{bmatrix} + \begin{bmatrix} D_1 \\ D_2 \end{bmatrix}\Gamma_C + \begin{bmatrix} H_1 \\ H_2 \end{bmatrix} w + \mathbf{m}. \tag{51b}$$

Our minimal representation is thus given by the upper row in equation (51*a*) and the lower row in (51*b*), i.e.,

$$\frac{d}{dt}\mathbf{X}'_a = \mathbf{A}_a\mathbf{X}'_a + \mathbf{B}_a\Gamma_C + \mathbf{G}_a w, \tag{52a}$$

$$Y_a \;\; = \mathbf{C}_a\mathbf{X}'_a + D_2\Gamma_C + H_2 w + m_2. \tag{52b}$$

We remark that the state vector in minimal representation (52*a*)–(52*b*) is expressed as $\mathbf{X}'_a = [x'_a \;\; y'_a]^T = \left[\frac{x'_1+x'_2}{2} \;\; \frac{y'_1+y'_2}{2}\right]^T$ which means that the new variables are simply averages of the original ones. Eigenvalue analysis of the matrices $\mathbf{A}_a$ and $\mathbf{A}_b$ reveals that $\mathbf{A}_a$ has two real eigenvalues (positive and negative) corresponding to the growing and decaying modes α and β, whereas the matrix $\mathbf{A}_b$ has a conjugate pair of purely imaginary eigenvalues which correspond to the neurally stable mode γ (Figure 6b). This observation allows us to conclude that the uncontrollable part of the system dynamics is associated with the neutrally stable oscillatory mode γ. In other words, the actuation (i.e., the cylinder rotation) can affect the growing and decaying modes (α and β), but has no authority over the neutrally stable mode γ. Consequently, original system (13*a*) is *stabilizable*, but is not *controllable*. As will be shown below, this fact will have important consequences when our linear control strategy is eventually applied to stabilize nonlinear Föppl system (11*a*).

We now proceed to discuss the synthesis of the control. The most common approach to solution of such problems offered by the control theory is the Linear–Quadratic–Gaussian (LQG) compensator. Construction of an LQG compensator is a standard result and we outline it below only briefly referring the reader to the classical monographs [1, 7] for further details. Assuming that all the stochastic variables w and $\mathbf{m}$ are white, zero–mean and Gaussian, the *separation principle* can be applied which means that the control and estimation problems can in fact be solved independently of each other. Based on the above assumptions, solution of the control problem can be further simplified by invoking the principle of *certainty equivalence* stating that the optimal feedback matrix $\mathbf{K}$ for stochastic system (13*a*) with cost function (43) is exactly the same as for deterministic system (12*a*)–(12*b*) with a corresponding cost functional (i.e., defined without the expectation). Since original system (13*a*) is not controllable, the optimal feedback matrix is determined as $\mathbf{K} = \begin{bmatrix}\mathbf{K}_a \\ \mathbf{0}\end{bmatrix}\mathbf{T}_c$, where $\mathbf{K}_a$ is the feedback matrix obtained for minimal representation (52*a*)– (52*b*). It is computed as

$$\mathbf{K}_a = \mathbf{R}^{-1}\mathbf{B}_a^T\mathbf{P} \tag{53}$$

in which the matrix $\mathbf{P}$ is a symmetric positive–definite solution of the *algebraic Riccati equation*

$$\mathbf{A}_a^T\mathbf{P} + \mathbf{P}\mathbf{A}_a + \mathbf{C}_{a0}^T\mathbf{Q}\mathbf{C}_{a0} - \mathbf{P}\mathbf{B}_a\mathbf{R}^{-1}\mathbf{B}_a^T\mathbf{P} = \mathbf{0}, \tag{54}$$

where $\mathbf{C}_{a0} = \begin{bmatrix}\mathbf{0} \\ \mathbf{C}_a\end{bmatrix}$. We note that the feedback matrix $\mathbf{K}_a$, and therefore also $\mathbf{K}$, will depend on the choice of the matrices $\mathbf{Q}$ and $\mathbf{R}$ weighting the system output and control in cost functional (43).

Since original system (13*a*)–(13*b*) with the observation operator given in (41) is completely observable, the estimation problem is solved based on full representation (13*a*)–(13*b*), rather than minimal representation (52*a*)–(52*b*). Thus, the optimal estimator feedback matrix needed in (44*a*) is given by

$$\mathbf{L} = \mathbf{S}\mathbf{C}^T\mathbf{M}^{-1}, \tag{55}$$

where the matrix **S** is a symmetric positive–definite solution of the algebraic Riccati equation

$$\mathbf{AS} + \mathbf{SA}^T + W\mathbf{GG}^T - \mathbf{SC}^T\mathbf{M}^{-1}\mathbf{CS} = \mathbf{0}, \tag{56}$$

in which the following disturbance structure is assumed $E[w(t)w(\tau)^T] = W\delta(t-\tau)$ and $E[\mathbf{m}(t)\mathbf{m}(\tau)^T] = \mathbf{M}\delta(t-\tau)$. Such estimator feedback gain **L**, depending on the covariances of the system and measurement disturbances W and **M**, yields an estimator known as the *Kalman filter* which is an optimal recursive filter designed to estimate the state of a dynamic system from a series of incomplete and noisy measurements [7]. The gain **L** blends the information from system model (13*a*) with actual measurements $\tilde{\mathbf{Y}}$ and is optimal in the sense that it minimizes the expected mean square estimation error $E[\|\mathbf{X}'(t) - \mathbf{X}_e(t)\|]$ for $t \to \infty$. Evidently, the key step required to determine the feedback gains **K** and **L** is solution of the algebraic Riccati equations, respectively, (54) and (56). For the case of the simple vortex system studied here these equations can be solved using standard techniques [112]. As a matter of fact, equation (54), corresponding to two–dimensional minimal representation (51*a*), represents a system of three coupled quadratic equations which can be reduced to a scalar quartic equation that, in principle, can be solved in a closed form. However, the analytical expressions obtained are extremely complicated and in practice it is much more convenient to use a numerical solution. The LQG compensator is an example of an $\mathcal{H}_2$ controller / estimator design in which disturbances are assumed Gaussian and uncorrelated with the state and control. Robustness of the compensator can be enhanced by performing an $\mathcal{H}_\infty$ controller / estimator design where disturbances are allowed to have the worst–case form [113]. In regard to the problem of determining an optimal value of x_m in (40) (i.e., the "sensor placement problem"), we remark that it can be solved, for instance, by choosing x_m to maximize the observability of the unstable mode α [108]. Finally, we mention that here the estimation problem is considered under the assumptions of an infinite time horizon and time–invariance of system (44*a*)–(44*b*). Solution of the estimation problem for vortex systems formulated in a more general setting will be discussed in Section 5.

We will now discuss some aspects of the application of the linear control strategy developed above to stabilize the original *nonlinear* problem (10). In order to make the mathematical analysis more tractable [110], instead of considering the LQG compensator, we will focus on the simpler case of the state–feedback controller (i.e., we drop the estimator, cf. Figure 15) applied to deterministic system (11*a*). Thus, setting $\mathbf{b}(\mathbf{X}) = -\mathbf{K}$ we can now rewrite (11*a*) as

$$\frac{d}{dt}\check{\mathbf{X}} = (\mathbf{A} - \mathbf{BK})\check{\mathbf{X}} + \mathbf{G}(\check{\mathbf{X}}), \tag{57}$$

where $\check{\mathbf{X}} \triangleq \mathbf{X} - \mathbf{X}_0$ is *not* assumed small and $\mathbf{G}(\check{\mathbf{X}}) \triangleq \mathbf{f}(\mathbf{X}_0 + \check{\mathbf{X}}) - \mathbf{A}\check{\mathbf{X}}$ [this change of variables shifts the equilibrium of system (11*a*) to the origin]. The fact that the uncontrollable mode γ is only *neutrally* stable has important consequences, both theoretical and practical, as regards the behavior of the closed–loop nonlinear system (57). As is well known (see, e.g., [87]), when the Jacobian of a nonlinear system calculated at an equilibrium has purely imaginary eigenvalues in addition to stable eigenvalues, it may not be possible to determine the local stability of this equilibrium based on this Jacobian alone. The reason is that in such situations

the leading–order behavior of the nonlinear system in a neighborhood of the equilibrium is determined by effects not captured in the Jacobian. Therefore, in order to characterize completely the behavior of system (57) near the origin we will take into account the nonlinear part $\mathbf{G}(\check{\mathbf{X}})$. We will prove below that the uncontrollable modes of system (12*a*) span in fact a center manifold of system (57). We begin by stating the Hamiltonian form of uncontrolled system (10). This representation will be needed below in the proof of the stability of the reduced system on the center manifold. As is well known (see, e.g., [102]), the Hamiltonian of two point vortices interacting with the free stream and the circular cylinder of unit radius is given by

$$\begin{aligned}\mathcal{H}(x_1,y_1,x_2,y_2) &= \frac{\Gamma^2}{4\pi}\ln|x_1^2+y_1^2-1| + \frac{\Gamma^2}{4\pi}\ln|x_2^2+y_2^2-1| + \frac{\Gamma^2}{2\pi}\ln\sqrt{(x_1-x_2)^2+(y_1-y_2)^2} \\ &-\frac{\Gamma^2}{2\pi}\ln\sqrt{1-2(x_1x_2+y_1y_2)+(x_1^2+y_1^2)(x_2^2+y_2^2)} - \Gamma\left(y_1-\frac{y_1}{x_1^2+y_1^2}\right)+\Gamma\left(y_2-\frac{y_2}{x_2^2+y_2^2}\right),\end{aligned} \tag{58}$$

so that equations of motion of the vortices (10) can be expressed as

$$\begin{cases} (-\Gamma)\dot{x}_1 = \dfrac{\partial\mathcal{H}}{\partial y_1}, \\ \Gamma\dot{x}_2 = \dfrac{\partial\mathcal{H}}{\partial y_2}, \\ (-\Gamma)\dot{y}_1 = -\dfrac{\partial\mathcal{H}}{\partial x_1}, \\ \Gamma\dot{y}_2 = -\dfrac{\partial\mathcal{H}}{\partial x_2}. \end{cases} \tag{59}$$

We now shift the equilibrium to the origin using the substitution $\mathbf{X} = \mathbf{X}_0 + \check{\mathbf{X}}$ and introduce the following *symplectic* transformation

$$\Xi = [\eta_1 \quad \xi_2 \quad \xi_1 \quad \eta_2]^T \triangleq \mathbf{Z}\check{\mathbf{X}} \tag{60}$$

defined by the matrix

$$\mathbf{Z} \triangleq \frac{1}{\sqrt{2}}\begin{bmatrix} 1 & 0 & -1 & 0 \\ 0 & 1 & 0 & -1 \\ 1 & 0 & 1 & 0 \\ 0 & 1 & 0 & 1 \end{bmatrix} \tag{61}$$

(the reason for the special ordering of the elements of the vector Ξ will become apparent below). As a result of these transformations, system (59) can be rewritten as

$$\begin{cases} \Gamma\dot{\eta}_1 = \dfrac{\partial\hat{\mathcal{H}}}{\partial\xi_1}, \\ \Gamma\dot{\xi}_2 = \dfrac{\partial\hat{\mathcal{H}}}{\partial\eta_2}, \\ \Gamma\dot{\xi}_1 = -\dfrac{\partial\hat{\mathcal{H}}}{\partial\eta_1}, \\ \Gamma\dot{\eta}_2 = -\dfrac{\partial\hat{\mathcal{H}}}{\partial\xi_2}, \end{cases}, \tag{62}$$

where the new Hamiltonian is $\hat{\mathcal{H}}(\Xi) \triangleq \mathcal{H}(\mathbf{X}_0 + \mathbf{Z}^T\Xi)$. We now remark that by exchanging the rows one and three in the matrix $\mathbf{Z}$ we in fact recover the transformation $\mathbf{T}_c$ [cf. (50)] introduced earlier in order to convert perturbation system (12*a*) to the minimal representation in which the controllable and uncontrollable parts are uncoupled. Hence, making this rearrangement in (62) and restoring the feedback control terms we can rewrite system (57) as

$$\frac{d}{dt}\begin{bmatrix} \xi \\ \eta \end{bmatrix} = \begin{bmatrix} \mathbf{A}_0 & 0 \\ 0 & \mathbf{A}_s \end{bmatrix}\begin{bmatrix} \xi \\ \eta \end{bmatrix} + \begin{bmatrix} \mathbf{g}_1(\xi,\eta) \\ \mathbf{g}_2(\xi,\eta) \end{bmatrix}, \tag{63}$$

where $\xi \triangleq [\xi_1 \;\; \xi_2]^T$ and $\eta \triangleq [\eta_1 \;\; \eta_2]^T$. The linear and nonlinear parts of system (63) are obtained as

$$\begin{bmatrix} \mathbf{A}_0 & 0 \\ 0 & \mathbf{A}_s \end{bmatrix} = \mathbf{T}(\mathbf{A} - \mathbf{B}\mathbf{K})\mathbf{T}^T, \tag{64}$$

$$\begin{bmatrix} \mathbf{g}_1(\xi,\eta) \\ \mathbf{g}_2(\xi,\eta) \end{bmatrix} = \mathbf{T}\mathbf{G}\left(\mathbf{T}^T\begin{bmatrix} \xi \\ \eta \end{bmatrix}\right). \tag{65}$$

The first row of (63) corresponds to the uncontrollable part of linearized system (12*a*) and the matrix $\mathbf{A}_0$ has a conjugate pair of purely imaginary eigenvalues, whereas the second row of (63) corresponds to the controllable part of system (12*a*) and, due to the effect of the feedback control term, the matrix $\mathbf{A}_s$ has eigenvalues with negative real parts only.

Transformation $\mathbf{T}_c$ splits the state space $\mathbb{R}^4$ into two subspaces W_c and W_s, i.e., $W_c \times W_s = \mathbb{R}^4$, such that $\xi \in W_c$ and $\eta \in W_s$. We now recall (see, e.g., [114]) that an *invariant* manifold, characterized by a smooth function $\Phi : W_c \to W_s$, is a set $\mathcal{M} \subset W_c$ such that if $\xi(0) \in \mathcal{M}$ and $\eta(0) = \Phi(\xi(0))$, then $\xi(t) \in \mathcal{M}$ and $\eta(t) = \Phi(\xi(t))$ for all times $t \in \mathbb{R}^+$. The following theorem, proven in [110], shows that system (63) has an invariant manifold with a particularly simple structure:

Theorem 2 *System (63) possesses an invariant manifold given by*

$$\Phi(\xi) = \begin{bmatrix} 0 \\ 0 \end{bmatrix}. \tag{66}$$

Thus, this invariant manifold coincides with the subspace W_c. We note that, since the matrix $\mathbf{A}_0$ has only purely imaginary eigenvalues, the invariant manifold is in fact a *center manifold* (see, e.g., [115]). Given (66), we can now perform an invariant reduction of system (63) and the reduced system on the center manifold is given by

$$\dot{\xi}_0 = \mathbf{A}_0\xi_0 + \mathbf{g}_1(\xi_0, \mathbf{0}). \tag{67}$$

We remark that application of the feedback control represented by the term $\mathbf{B}\mathbf{K}\check{\mathbf{X}}$ in (57), while stabilizing locally this system, may in general break its Hamiltonian structure. However, we recall that $\mathbf{T}$ represents a transformation to the minimal representation, so that

$$\mathbf{T}\mathbf{B}\mathbf{K}\mathbf{T}^T = \begin{bmatrix} 0 & 0 \\ 0 & \mathbf{B}_0\mathbf{K}_0 \end{bmatrix},$$

where $\mathbf{B}_0\mathbf{K}_0$ is a 2×2 block. This, together with Theorem 2, implies that reduced system (67) is in fact invariant with respect to the feedback control. This observation will play an important role in the assertion that reduced system (67) has in fact periodic solutions and that its origin is stable. The first part of this result is made precise in the following theorem proven in [110]:

Theorem 3 *Reduced system (67) has a one–parameter family of closed orbits (periodic solutions) in a open neighborhood of the origin.*

The reduced Hamiltonian $\hat{\mathcal{H}}_0(\xi_1,\xi_2) \triangleq \hat{\mathcal{H}}(0,\xi_2,\xi_1,0)$ may thus serve, after some trivial modifications, as the Lyapunov function for system (67) and its invariance along the trajectories implies stability of the origin. We conclude this part by stating a corollary, also proven in [110], addressing the stability of the fully nonlinear Föppl system with feedback control:

Corollary 1 *For initial conditions sufficiently close to equilibrium (15), solutions of the closed–loop Föppl system (57) converge as $t\to\infty$ to periodic orbits.*

We are now ready to analyze computational results illustrating the application of the LQG compensator to stabilize equilibrium (15) of the Föppl system. In investigations [108, 111] the downstream coordinate of this equilibrium was chosen as $x_0 = 4.32$ which ensures that the length of the recirculation bubble in the Föppl potential flow is the same as in the unstable equilibrium solution of the Navier–Stokes system at $Re = 75$ [116]. In Figure 16a we show the trajectories of the vortices in system (10), i.e., without the control, as they escape to infinity when the equilibrium $\mathbf{X}_0$ is perturbed with a small perturbation $\mathbf{X}'(0)$. We remark that the directions along which the initial escape takes place are in qualitative agreement with the unstable eigendirections shown schematically in Figure 6b. In Figure 16b,c we show how the system evolution resulting from the same perturbation is stabilized by the LQG compensator. In Figure 16c we also show the corresponding estimator trajectory $\mathbf{X}_e(t) \triangleq \mathbf{X}_0 + \mathbf{X}'_e(t)$ which starts from the equilibrium $\mathbf{X}_0$ and then, after some transient, rapidly converges to the actual system trajectory $\mathbf{X}(t)$. We remark that, while the action of the LQG compensator prevents the state of the system from escaping to infinity, it does not succeed in stabilizing asymptotically the equilibrium $\mathbf{X}_0$. Instead, the state of the system lands on a circular trajectory which circumscribes the equilibrium (Figure 16c). This circular orbit is precisely the center manifold whose existence and properties were stipulated by Theorems 2 and 3. Thus, we see that, in agreement with Corollary 1, the long–time behavior of the controlled system is determined by the properties of reduced system (67) on the center manifold which was proved to sustain, for bounded initial data, periodic oscillations. We emphasize also that, as is evident from Figure 16b,c, the LQG compensator is able to stabilize the system for fairly significant magnitudes of the initial perturbation $\mathbf{X}'(0)$.

As was also done in several other studies discussed in the present review [98, 101, 106, 107], the controller derived based on an inviscid vortex dynamics model was subsequently applied to stabilize a viscous fluid flow governed by the Navier–Stokes system. In the context of the LQG compensator this was done by replacing nonlinear Föppl system (10) with a Navier–Stokes solver as the "plant" (cf. Figure 15). A sample vorticity field, obtained at the

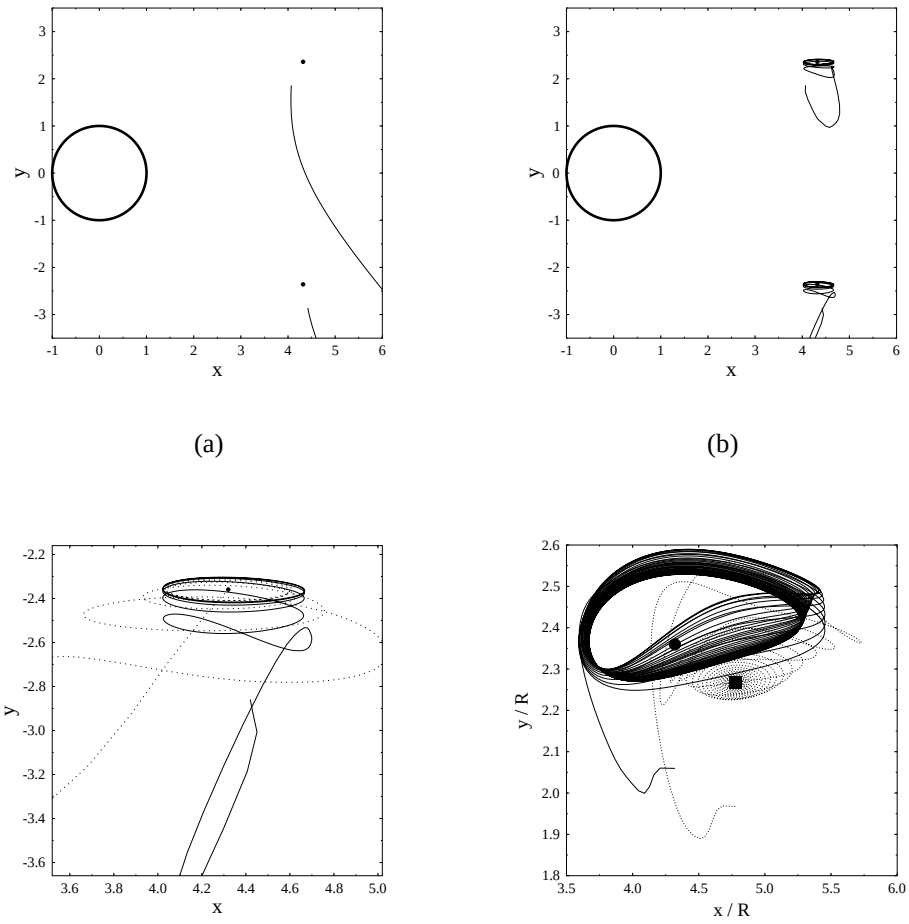

Figure 16. Trajectories of the vortices in the Föppl system resulting from a small perturbation of equilibrium: (a) uncontrolled case, (b) case with control performed by the LQG compensator (57), (c) same as (b), but showing magnification of the neighborhood of the lower equilibrium locus; in Figure (c) the dotted line represents the corresponding estimate $\mathbf{X}_e(t)$ of the vortex trajectory; the equilibrium points are indicated by solid circles, (d) trajectories of the state of (solid line) the classical and (dotted line) higher–order Föppl system stabilized with an LQG compensator in the neighborhood of the corresponding equilibrium solutions [111].

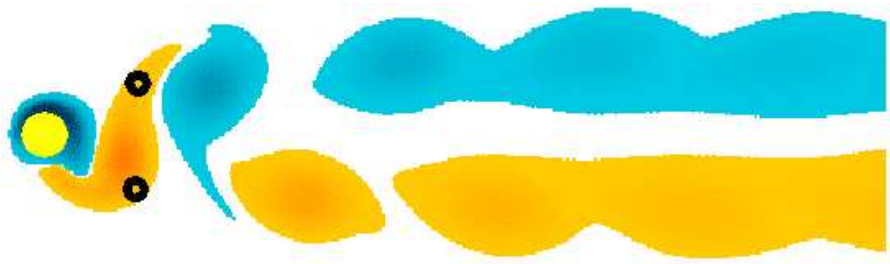

Figure 17. The vorticity field in a viscous wake flow at $Re = 75$ under the action of the LQG compensator. The black circles represent the instantaneous positions of the Föppl vortices estimated by the Kalman filter based on velocity measurements [108]. (multimedia animation)

Reynolds number $Re = 75$ some time after the LQG compensator was turned on, is shown in Figure 17 [108]. We remark that the downstream part of the wake is remarkably symmetrized by the action of the compensator. On the other hand, the level of the velocity fluctuations in the part of the flow close to the cylinder was in fact increased, as was the average drag force [108]. We emphasize that in this case too the time evolution of the Föppl vortices as estimated by the Kalman filter also exhibits the center manifold behavior already observed in Figure 16b,c.

Evidently, solution of the Riccati equation, either the one associated with the controller [cf. (54)], or the one associated with the estimator [cf. (56)], requires storage of order $O(N^2)$. Thus, when the system model is high–dimensional, as are those resulting, for example, from discretizations used in the direct numerical simulations (DNS) of high–Reynolds number turbulent flows, determination of the feedback kernels becomes computationally intractable. This motivates the pursuit of vortex models which, while remaining low–dimensional, could approximate infinite–dimensional solutions of Euler equations with desired accuracy. As an example of such a model we developed the family of the higher–order Föppl systems discussed in Section 2.4. Remarkably, the uncontrollable modes of the linearizations of the higher–order Föppl systems around their equilibria *are* asymptotically stable. Consequently, the center manifold behavior is no longer present in higher–order Föppl systems with a linear feedback stabilization, and therefore the higher–order equilibria z_{N_0} can now be *asymptotically* stabilized by an LQG compensator (Figure 16d). The disappearance of the center–manifold behavior results from the fact that purely imaginary eigenvalues are a structurally unstable property of a linear operator which is not preserved when this operator is perturbed in an arbitrary manner.

We now proceed to discuss the work of Iollo and Zannetti [120, 121] who employed the methods of adjoint–based optimization to control vortices trapped in cavities. These investigations were motivated by the problem of stability of the high–lift vortex configurations discussed earlier in Section 2.4. While both investigations used unsteady mass transpiration, modeled by a point source / sink, as the actuation, the study [120] focused on the generic case of a cornice–shaped cavity on an unbounded flat wall, whereas the study [121] specialized these results for the case of a cavity on the surface of a modified Joukowski airfoil. In both cases the vortex equilibrium located inside the cavity is neutrally stable and the control problem consisted in determining a time–dependent sink / source intensity $\Lambda : [t_1, t_2] \to \mathbb{R}$ that, given an initial perturbation of the vortex position away from the equilibrium $\mathbf{X}_0$, will bring the vortex back to the equilibrium location. The optimal control $\mathbf{U}^{opt} = \Lambda^{opt}$ was determined by solving a minimization problem of the type (1), where the cost functional

$$\mathcal{J}(\Lambda) = j(\mathbf{X}(\Lambda), \Lambda) = \frac{1}{2} \int_{t_1}^{t_2} \|\mathbf{X}(t) - \mathbf{X}_0\|^2 \, dt \tag{68}$$

represents the integrated distance of the actual vortex position $\mathbf{X}(t)$ from the equilibrium $\mathbf{X}_0$, whereas the constraint equation $\mathbf{E}(\mathbf{X}, \Lambda) = \mathbf{0}$ is given by governing system (11*a*). The optimal control Λ^{opt} and the corresponding optimal trajectory $\mathbf{X}^{opt} \triangleq \mathbf{X}(\Lambda^{opt})$ can be characterized using the method of the Lagrange multipliers [7]. Defining an *adjoint* state $\lambda : [t_1, t_2] \to \mathbb{R}^N$, we can construct the Lagrangian $\mathcal{L}(\mathbf{X}, \Lambda, \lambda)$ by augmenting cost functional (68) with the

constraint equation as follows

$$\mathcal{L}(\mathbf{X},\Lambda,\lambda) \triangleq j(\mathbf{X},\Lambda) + \int_{t_1}^{t_2} \lambda^T \cdot \left(\frac{d\mathbf{X}}{dt} - \mathbf{f}(\mathbf{X}) - \mathbf{b}(\mathbf{X})\Lambda \right) dt. \tag{69}$$

The optimal control Λ^{opt}, the optimal trajectory $\mathbf{X}^{opt}$ and the adjoint state λ are then determined by the following conditions

$$\frac{\partial \mathcal{L}}{\partial \Lambda}(\mathbf{X}^{opt},\Lambda^{opt},\lambda^{opt}) = 0 \quad \Longrightarrow \quad \mathbf{b}(\mathbf{X}^{opt})\lambda = 0, \tag{70}$$

$$\frac{\partial \mathcal{L}}{\partial \mathbf{X}}(\mathbf{X}^{opt},\Lambda^{opt},\lambda^{opt}) = 0 \quad \Longrightarrow \quad -\frac{d\lambda}{dt} - \left[\nabla \mathbf{f}(\mathbf{X}^{opt})\right]^T \lambda = -\mathbf{X}^{opt} - \mathbf{X}_0 \tag{71}$$

$$\frac{\partial \mathcal{L}}{\partial \lambda}(\mathbf{X}^{opt},\Lambda^{opt},\lambda^{opt}) = 0 \quad \Longrightarrow \quad \frac{d\mathbf{X}^{opt}}{dt} - \mathbf{f}(\mathbf{X}^{opt}) - \mathbf{b}(\mathbf{X}^{opt})\Lambda^{opt} = \mathbf{0}, \tag{72}$$

where Equation (71) is supplemented with a terminal condition $\lambda(t_2) = \mathbf{0}$, whereas Equation (72) is supplemented with an initial condition $\mathbf{X}(t_1) = \mathbf{X}_P$, with $\mathbf{X}_P$ denoting the initial perturbed position of the vortex. We emphasize that the partial derivatives on the LHS in (70)–(72) are to be understood in the sense of Fréchet and the RHS in (70)–(72) are defined for (almost) all $t \in [t_1,t_2]$. Since solution of system (70)–(72) in one shot is usually impossible, the optimal control Λ^{opt} can be determined using an iterative gradient–based descent algorithm

$$\Lambda^{(k+1)} = \Lambda^{(k)} - \tau^{(k)} \nabla \mathcal{J}(\Lambda^{(k)}), \;\; k = 0,1,\ldots \tag{73}$$

as $\Lambda^{opt}(t) = \lim_{k\to\infty} \Lambda^{(k)}(t)$, where k is the iteration count, $\Lambda^{(0)}(t)$ is an initial guess for the control and $\tau^{(k)}$ is the length of the step in the descent direction (in practice, one may use a more advanced version of algorithm (73), such as, e.g., the conjugate gradients method, or a variant of the quasi–Newton method [122]). A critical element of descent algorithm (73) is determination of the cost functional gradient $\nabla \mathcal{J}(\Lambda^{(k)})$. As a matter of fact, it can be conveniently expressed in terms of the adjoint and state variables as

$$\nabla \mathcal{J}(\Lambda^{(k)}(t)) = \mathbf{b}(\mathbf{X}^{(k)}(t))\lambda^{(k)}(t), \qquad t \in [t_1,t_2]. \tag{74}$$

Relationship (74) illustrates the important fact that away from the saddle point characterized by (70)–(72), the adjoint variables (i.e., the Lagrange multipliers) encode information about the *sensitivities* of cost functional (68) to perturbations of the control Λ. We remark that $\lambda = \lambda(t)$ is given as a solution of adjoint system (71) which is a *terminal* value problem and, as such, has to be integrated *backwards* in time. This is a standard approach to computational solution of optimization problems constrained by differential equations and we refer the reader to the monograph [10] for an in–depth discussion. A sample result from [121] is presented in Figure 5b which illustrates the convergence of the point vortex from some initial perturbed position $\mathbf{X}_P$ (P) to the equilibrium $\mathbf{X}_0$ (S) under the action of the optimal control $\Lambda^{opt}(t)$. As recognized by the authors, this vortex model suffers from the limitation that a system with the vortex perturbed away from the equilibrium no longer satisfies the Kutta condition.

We conclude this Section by discussing the recent investigations by Shashikanth et al. [117, 118] who considered the control of a more general problem, namely, when the cylinder is allowed to move freely in response to the forces exerted on it by the fluid with N vortices in it, thereby mimicking a fluid–structure interaction problem. These investigations rely on a

compact Hamiltonian description of the coupled system, comprised of the cylinder and all N vortices, which was developed earlier in [84] and revisited recently in [119]. The actuation is assumed to have the form of a force applied to the center of mass of the cylinder and have magnitude constrained by a lower and upper bound, U_{min} and U_{max}, respectively. As compared to the problems considered above, this problem is made more complicated by the presence of inequality constraints on the control $\mathbf{U}$. As a result, in particular the adjoint–based optimization approach of Iollo and Zannetti [121, 120] is inapplicable, and more general methods, such as Pontryagin's maximum principle [6] need to be employed. Thus, after rewriting the governing system in a form consistent with (11a), the authors analyzed in [117] the properties of the optimal control $\mathbf{U}^{opt}$ determined using Pontryagin's technique, i.e., as

$$\mathbf{U}^{opt} = \text{argmax}_{\mathbf{U}} \mathcal{H}_P(\mathbf{X}, \mathbf{U}, \lambda), \tag{75}$$

where $\mathcal{H}_P(\mathbf{X}, \mathbf{U}, \lambda) \triangleq \lambda^T \mathbf{f}(\mathbf{X}) + \lambda^T \mathbf{b}(\mathbf{X})\mathbf{U} + \lambda_0 f_0$ is Pontryagin's Hamiltonian with $\lambda \in \mathbb{R}^N$ and $\lambda_0 \in \mathbb{R}$ denoting the adjoint variables and the cost functional is given by $\mathcal{J}(\mathbf{X}, \mathbf{U}) = \int_{t_1}^{t_2} f_0(t, \mathbf{X}(t), \mathbf{U}(t))\, dt$. Considering the point–to–point transfer problem (corresponding to $f_0 \equiv 1$), in [117] the authors used methods of the geometric control to study general conditions under which the optimal control will be of the "bang–bang" type, i.e., switching between the lower and upper bounds U_{min} and U_{max}. In [118] the author used the methods of Hamiltonian mechanics to obtain reduced descriptions of the same system which made it then possible to develop expressions for controllers designed to alter the vortex orbit from the bound to the scattering type and vice versa.

5. Estimation of Vortex Flows

In this Section we discuss the problem of *state estimation* for vortex systems, i.e., the problem of determining the state of the system $\mathbf{X}(t)$ based on some incomplete and possibly noisy measurements obtained via (12b). Since most feedback control algorithms require full state information, such estimation methods are necessary in practice when partial measurements are only available. In most situations, the goal is to use measurements of velocity [cf. (40)], or pressure in the flow domain, or on the domain boundaries, to estimate the positions $z_1, \ldots, z_N$ of the vortices in the system. While this problem has already been partially addressed in Section 4.2 in the context of the Föppl system, here we seek to present a more complete picture. A first attempt at solving the estimation problem for a vortex system was made by Cortelezzi et al. in the study [96] concerning the control of a vortex interacting with a semi–infinite plate (Figure 10a). Based on an analysis of the velocity signature at the plate, the authors showed that the position of the vortex could be uniquely determined using measurements of the Y–component of the velocity and its derivative at the tip of the plate. Then, the vortex circulation Γ can be determined using the Kutta condition. This setting, however, represents a rather simple situation in which the measurements are "complete", in the sense that their number matches the number of degrees of freedom (i.e., 2) and they are not contaminated by noise. In such situations an exact reconstruction is possible at every instant of time.

A more complicated problem, from the point of view of the estimation theory, was considered by Anderson et al. in [100] where the authors used system identification techniques to construct an approximate mathematical model for the input–output map in a higher–order vortex model proposed in [98]. The input for the system has the form of suction at the base of the plate $\mathbf{U}(t) = \Lambda(t)$, whereas the output has the form of the velocity measurements given in (33). The system identification method used in [100] was the auto–regressive model with exogenous input (ARX) defined by the formula

$$\mathbf{Y}(t) + \sum_{l=1}^{n} a_l \mathbf{Y}(t - l\Delta t) = \sum_{l=1}^{n} b_l \mathbf{U}(t - l\Delta t), \tag{76}$$

where n is the order of the model and $\{a_l, b_l\}_{l=1}^{n}$ are coefficients determined by performing a least–squares fit to the data. The ARX model is a technique for constructing a mathematical description of a process based on measured data which accounts also for the presence of a zero–mean white noise in the measurements. The data necessary to identify the coefficients in input–output relation (76) was obtained by actuating the vortex system with zero–mean white noise as the control $\mathbf{U}$. An optimal value of the order of the model was determined by requiring that it give the most accurate L_2 system response to harmonic input with a range of frequencies. The ARX model of the input–output map for the vortex system was thoroughly validated which included analysis of the frequency response, mean value ("DC gain") response and step response.

The state estimation problem was also considered in investigation [93] concerning the control of the "corner flow" (Figure 9). In that study the observation operator corresponded to the measurements of the tangential velocity component at a boundary point $z_m = x_m + \mathrm{i}0$

$$\mathbf{Y} \triangleq \left[\; \Re[V(x_m)] \; \right] + \mathbf{D}\Gamma_C, \tag{77}$$

where $\mathbf{D} = [kx_m]$ represents the feed–through effect of the control on the measurements. The estimation problem was solved in [93] using the governing system written in terms of flat coordinates (30) and employing the method developed earlier in [123]. This approach is based on deriving an estimator system corresponding to (30), namely

$$\frac{d}{dt}\begin{bmatrix} \hat{z}_1 \\ \hat{z}_2 \end{bmatrix} = \begin{bmatrix} \hat{z}_2 \\ p(\hat{z}_1, \hat{z}_2) \end{bmatrix} + \begin{bmatrix} 0 \\ q(\hat{z}_1, \hat{z}_2) \end{bmatrix} \mathbf{U} + \begin{bmatrix} L_1 \\ L_2 \end{bmatrix} (\mathbf{Y} - \tilde{\mathbf{Y}}), \tag{78}$$

where $\hat{z}_1$ and $\hat{z}_2$ are estimates of the flat coordinates z_1 and z_2, $\mathbf{L} = [L_1 \;\; L_2]^T$ is the feedback operator, whereas $(\mathbf{Y} - \tilde{\mathbf{Y}})$ represents the difference between the actual and estimated measurements. The feedback gains L_1 and L_2 are chosen to ensure that the linearization of (78) around the equilibrium is stable, so that the estimation errors $(\hat{z}_1 - z_1)$ and $(\hat{z}_2 - z_2)$ decrease with time if the initial estimates $\hat{z}_1$ and $\hat{z}_2$ are sufficiently good. While this approach does not guarantee the optimality of the estimates in any sense, the computational results reported in [123, 93] showed good performance of the estimator in a neighborhood of the equilibrium.

A solution to the state estimation problem for an LTI system that is optimal in the sense that $E[\|\mathbf{X}'(t) - \mathbf{X}'_e(t)\|] = \min$ for $t \to \infty$ can be obtained using the Kalman filter. Such an approach, developed in the context of a vortex stabilization problem in [108], was already

discussed in Section 4.2, and here we present some extensions of this idea. A more general problem of state estimation for vortex systems was considered in [124, 125] where the authors used an *Extended Kalman Filter* (EKF) over a sliding time window $[t,t+T]$ [7]. EKF is usually used in the time–discrete setting and consists of the following steps

(i) *Dynamic forecast:*

$$\bar{\mathbf{X}}_e(t+\Delta t) = \mathbf{X}_e t + \Delta t \mathbf{f}(\mathbf{X}_e(t)) + \Delta t \mathbf{b}(\mathbf{X}_e(t))\mathbf{U}(t), \tag{79}$$

$$\bar{\mathbf{P}}_e(t+\Delta t) = \mathbf{A}(t)\mathbf{P}_e(t) + \mathbf{P}_e(t)[\mathbf{A}(t)]^T + \mathbf{Q}, \tag{80}$$

where $\mathbf{A}(t) \triangleq \nabla \mathbf{f}(\mathbf{X}_e(t))$ is the Jacobian of $\mathbf{f}$ computed at a specific trajectory $\mathbf{X}_e(t)$. Here we use system model (11*a*) to advance the state estimate $\mathbf{X}_e$ and its error covariance $\mathbf{P}_e$ over one time step from t to $t+\Delta t$. We note that in the extended Kalman filter equation (79), but not (80), uses the nonlinear function $\mathbf{f}(\mathbf{X}_e)$, rather than its linearization $\mathbf{A}$.

(ii) *Update:*

$$\mathbf{X}_e(t+\Delta t) = \bar{\mathbf{X}}_e(t+\Delta t) + \mathbf{L}(t+\Delta t)\left[\tilde{\mathbf{Y}}(t+\Delta t) - \mathbf{c}(\bar{\mathbf{X}}_e(t+\Delta t))\right], \tag{81}$$

$$\mathbf{P}_e(t+\Delta t) = \bar{\mathbf{P}}_e(t+\Delta t) - \mathbf{L}(t+\Delta t)\mathbf{C}(t+\Delta t)\bar{\mathbf{P}}_e(t+\Delta t), \tag{82}$$

where $\mathbf{C}(t+\Delta t) = \nabla \mathbf{c}(\mathbf{X}_e(t+\Delta t))$ is the Jacobian of the observation operator $\mathbf{c}$ computed at a specific trajectory $\mathbf{X}_e$ and the time–dependent feedback gain is obtained as

$$\mathbf{L}(t+\Delta t) = \mathbf{P}_e(t+\Delta t)[\mathbf{C}(t+\Delta t)]^T \left\{\mathbf{C}(t+\Delta t)\mathbf{P}_e(t+\Delta t)[\mathbf{C}(t+\Delta t)]^T + \mathbf{R}\right\}^{-1}. \tag{83}$$

Here one uses the actual measurements $\tilde{\mathbf{Y}}$ to update the state estimate $\mathbf{X}_e$ and, in the spirit of the extended Kalman filter, in (81) the nonlinear observation operator $\mathbf{c}$ is used instead of its linearization $\mathbf{C}$.

While EKT does not ensure optimality of the estimate, it is the most commonly used estimator for nonlinear problems. The investigations [124, 125] demonstrated the possibility of using EKF to solve the estimation problem for systems consisting of two and four vortices with measurements $\tilde{\mathbf{Y}}$ in the form of Lagrangian tracer positions. Another application of EKF to a vortex dynamics problem was developed in [88] and concerned the vortex pair problem considered in [85] and discussed in Section 3 of the present paper. In [85, 88] the system measurements were also assumed in the form (40) with the velocity components recorded at a point $z_m = 0 + \mathrm{i}0$. Assuming a sliding temporal window $[t-T,t]$, the measurements $\tilde{\mathbf{Y}}$ were expanded as

$$\tilde{\mathbf{Y}}(t+\tau) = \mathbf{a}_0 + \sum_l \mathbf{a}_l \cos(l\varpi\tau) + \mathbf{b}_l \sin(l\varpi\tau), \tag{84}$$

where $\tau \in [t-T,t]$, ϖ is the instantaneous frequency and $T = \frac{2\pi}{\varpi}$. The estimation problem in [88] was then formulated in terms of the *phasors* $\mathbf{a}_l$ and $\mathbf{b}_l$ corresponding to the dominating harmonics. This problem was solved using an EKF approach given by (79)–(80) and (81)–(82), and the computational results demonstrated the applicability of the extended Kalman filtering technique to the considered estimation problem for a point vortex system.

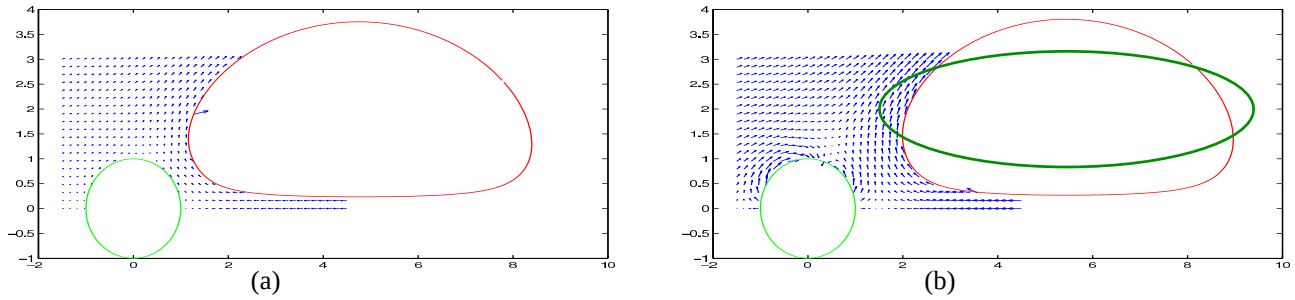

Figure 18. Prandtl–Batchelor solutions of Euler equation (2) with the RHS given by (14) corresponding to (a) homogeneous and (b) nonhomogeneous velocity boundary conditions. The thick line in Figure (b) represents a possible target shape of the vortex region A in the optimization problem.

6. Towards Optimal Control of Flows with Finite–Area Vortices

Most of the discussion presented in Sections 3 and 4 concerned control and estimation of point vortex systems and, as such, was motivated by the need to reduce the dimensionality of the flow model, making it possible in this way to apply methods of the control theory in a straightforward manner. In the present Section we would actually like to step outside this paradigm and revisit solutions of Euler equation (2) discussed in Section 2.4. More specifically, we will formulate an optimal control problem for the family of Prandtl–Batchelor flows [61] depicted in Figure 2 (top row, second column). This problems remain a subject of the current research and below we only outline a solution strategy highlighting some novel mathematical ingredients required to solve such problems. We remark that passive control of rotating finite–area vortex regions in unbounded domains, the so–called "V–states" [126], was considered by Friedland et al. [127, 128, 129] who used a time–dependent external strain field as the actuation to obtain autoresonance conditions. In Figure 18 we present two solutions of problem (2) featuring the Prandtl–Batchelor vortices: the solution in Figure 18a corresponds to the homogeneous velocity boundary conditions in (2), i.e., $\mathbf{u}\cdot\mathbf{n}|_\Sigma = \frac{\partial\psi_b}{\partial s}|_\Sigma = 0$, whereas the solution in Figure 18b corresponds to an arbitrarily selected wall transpiration given by $\mathbf{u}\cdot\mathbf{n}|_\Sigma = \frac{\partial\psi_b}{\partial s}|_\Sigma = \frac{1}{2}U_\infty\cos(2\theta)$. The symbol Σ denotes the part of the domain boundary (i.e., the surface of the obstacle) where the control is applied ($\Sigma\subseteq\partial\Omega$), whereas θ is the azimuthal angle in the polar coordinates. We note that, as a result of this passive actuation, the shape and location of the vortex region A is significantly changed. The control problem we propose consists in determining the distribution of the wall–normal velocity $\mathbf{u}\cdot\mathbf{n}|_\Sigma$, or equivalently the streamfunction ψ_b, such that the vortex region will have a prescribed shape, e.g., the shape indicated with a thick line in Figure 18b. Given the importance of vorticity for mixing processes (see, e.g., [130]), such a problem is relevant to optimization of regions where mixing occurs in high–Re flows. Moreover, the mathematical tools required to solve this problem are also representative of a broad family of similar problems. Denoting $\Delta A(\psi_b)$ the region enclosed between the prescribed and actual patch boundaries, we state this problem as follows

[cf. (1)]

$$\begin{aligned} &\min_{\psi,\psi_b} j(\psi,\psi_b), \\ &\text{subject to Equation } (2), \end{aligned} \tag{85}$$

where

$$j(\psi,\psi_b) = \frac{1}{2}\int\int_{\Delta A(\psi_b)} dxdy \tag{86}$$

is the area of the region $\Delta A(\psi_b)$. While this problem can be solved using the method of Lagrange multipliers described in Section 4.2 [cf. (68)–(72)], for illustration purposes we adopt here an alternative approach that has been frequently used in the context of flow control problem (in the continuous setting the two formulations are equivalent and lead to the same solution). Since from (2) we have $\psi = \psi(\psi_b)$, we can eliminate the state variable ψ from the cost functional $j(\psi,\psi_b)$ by defining a *reduced* cost functional $\mathcal{J}(\psi_b) \triangleq j(\psi(\psi_b),\psi_b)$, so that constrained minimization problem (85) can be replaced with an unconstrained one

$$\min_{\psi_b} \mathcal{J}(\psi_b). \tag{87}$$

A local minimizer ψ_b^{opt} of problem (87) is characterized by the vanishing of the Gâteaux differential, defined as $\mathcal{J}'(\psi_b;\psi_b') \triangleq \lim_{\varepsilon\to 0}\frac{1}{\varepsilon}[\mathcal{J}(\psi_b+\varepsilon\psi_b') - \mathcal{J}(\psi_b)]$ where ψ_b' is an arbitrary perturbation, of the cost functional $\mathcal{J}(\psi_b)$ as

$$\forall_{\psi_b'} \;\; \mathcal{J}'(\psi_b^{opt};\psi_b') = 0. \tag{88}$$

Differentiation of expressions such as (86) with respect to ψ_b is a delicate matter, because the area $\Delta A(\psi_b)$ is defined by the boundary of the vortex region A coinciding with a level set of the solution of Euler equation (2). Rewriting (2) with RHS (14) in the following equivalent form

$$|A(\psi_b)|\Delta\psi_1 = \Gamma \qquad \text{in } A(\psi_b), \tag{89}$$

$$\Delta\psi_2 = 0 \qquad \text{in } \Omega\backslash A(\psi_b), \tag{90}$$

$$\psi_1 = \psi_2 = \psi_0 \qquad \text{on } \partial A(\psi_b), \tag{91}$$

$$\frac{\partial\psi_1}{\partial n} = \frac{\partial\psi_2}{\partial n} \qquad \text{on } \partial A(\psi_b), \tag{92}$$

$$\psi_2 = \psi_b \qquad \text{on } \partial\Omega \tag{93}$$

where $\psi_1 = \psi|_{A(\psi_b)}$ and $\psi_2 = \psi|_{\Omega\backslash A(\psi_b)}$ are the solutions defined, respectively, in the interior and exterior of the vortex region, it is evident that system (2) with (14) is in fact a *free–boundary* problem, i.e., one in which the internal boundary ∂A separating the two subdomains needs to be determined as a part of the solution of the problem. Differentiation of such equations with respect to a parameter such as the boundary condition ψ_b requires care, because perturbing ψ_b also changes the *location* where boundary conditions (91)–(92) are imposed. A suite of mathematical techniques making it possible to differentiate solutions of PDEs defined in variable domains is referred to as the *shape differential* calculus [131]. We will use below a number of specific results belonging to the shape differential calculus to re–express

the Gâteaux differential $\mathcal{J}'(\psi_b;\psi_b')$, and refer the reader to the original source for derivation details. Thus, this Gâteaux differential can be computed as

$$\mathcal{J}'(\psi_b;\psi_b') = \oint_{\partial A(\psi_b)} \mathbf{z}(\psi_b;\psi_b')\cdot\mathbf{n}\,d\sigma = -\oint_{\partial A(\psi_b)} \frac{\psi'}{\frac{\partial\psi}{\partial n}}\bigg|_{\partial A(\psi_b)} d\sigma, \tag{94}$$

where $\mathbf{z}(\psi_b;\psi_b')$ is the perturbation (displacement) of the boundary $\partial A(\psi_b)$ and ψ' the perturbation of ψ obtained as a result of perturbing the boundary condition ψ_b with ψ_b'. The last term in (94) arises from the shape differentiation of Dirichlet boundary condition (91) as follows [131]

$$\frac{d\psi}{d\psi_b}\bigg|_{\partial A(\psi_b)} = \psi'|_{\partial A(\psi_b)} + \frac{\partial\psi}{\partial n}\bigg|_{\partial A(\psi_b)}(\mathbf{z}\cdot\mathbf{n}) = \frac{d\psi_0}{d\psi_b} = 0. \tag{95}$$

The perturbation variable ψ' satisfies the following linear PDE obtained from shape–differentiation of (2) with (14), or equivalently (89)–(93)

$$\begin{aligned}
\mathcal{L}\psi' \triangleq |A(\psi_b)|\Delta\psi' - \frac{\Gamma}{\frac{\partial\psi}{\partial n}\Big|_{\partial A(\psi_b)}}\delta\left(\mathbf{x}-\mathbf{x}|_{\partial A(\psi_b)}\right)\psi' \\
+ \frac{\Gamma}{|A(\psi_b)|}\left(\oint_{\partial A(\psi_b)} \frac{\psi'}{\frac{\partial\psi}{\partial n}}\bigg|_{\partial A(\psi_b)} d\sigma\right) H(\psi_0-\psi) = 0, \qquad \text{in } \Omega \qquad (96)\\
\psi' = \psi_b' \qquad \text{on } \partial\Omega.
\end{aligned}$$

Note that for convenience this system is now written in the whole domain Ω. Our goal now is to identify the gradient $\nabla\mathcal{J} : \Sigma \to \mathbb{R}$ is the cost functional $\mathcal{J}(\psi_b)$ with respect to the boundary condition ψ_b, so that we would use it in an iterative minimization algorithm as described in Section 4.2 [cf. (73)]. Existence of such gradient is guaranteed by the Riesz theorem [132] which, under the assumption of square integrability of ψ_b, allows one to re–express the Gâteaux differential as follows

$$\mathcal{J}'(\psi_b;\psi_b') = \left(\nabla\mathcal{J},\psi_b'\right)_{L_2(\Sigma)} = \int_\Sigma \nabla\mathcal{J}\,\psi_b'\,d\sigma, \tag{97}$$

where $(\cdot,\cdot)_{L_2(\Sigma)}$ is an L_2 inner product of functions defined on the cylinder boundary Σ. Representation (94) is, however, incompatible with (97), because the perturbation variable ψ_b' is hidden in the boundary condition for problem (96). Expression (94) can be transformed into a suitable form by introducing an *adjoint* state $\psi^* : \Omega \to \mathbb{R}$ and using the following identify

$$\left(\mathcal{L}\psi',\psi^*\right)_{L_2(\Omega)} = \left(\psi',\mathcal{L}^*\psi^*\right)_{L_2(\Omega)} + b \tag{98}$$

where the adjoint operator $\mathcal{L}^*\psi^*$ is defined as

$$\begin{aligned}
\mathcal{L}^*\psi^* \quad &\triangleq |A(\psi_b)|\Delta\psi^* + \frac{\Gamma}{\frac{\partial\psi}{\partial n}\Big|_{\partial A(\psi_b)}}\left(\frac{\int_{A(\psi_b)}\psi^*\,d\Omega}{|A(\psi_b)|} + \psi^*\right)\delta\left(\mathbf{x}-\mathbf{x}|_{\partial A(\psi_b)}\right)\\
&= \frac{|A(\psi_b)|}{\frac{\partial\psi}{\partial n}\Big|_{\partial A(\psi_b)}}\delta\left(\mathbf{x}-\mathbf{x}|_{\partial A(\psi_b)}\right), \qquad \text{in } \Omega \qquad (99)\\
&\psi^* = 0 \qquad \text{on } \partial\Omega.
\end{aligned}$$

Performing integration by parts implied by identity (98) yields the following form of the term b

$$b = -\oint_{\partial A(\psi_b)} \frac{\psi'}{\frac{\partial \psi}{\partial n}}\bigg|_{\partial A(\psi_b)} d\sigma - \int_\Sigma \psi_b' \frac{\partial \psi^*}{\partial n} d\sigma = 0 \tag{100}$$

from which, by noting (94) and (97), we finally obtain a simple expression for the cost functional gradient

$$\nabla \mathcal{J} = \frac{\partial \psi^*}{\partial n}\bigg|_\Sigma. \tag{101}$$

This gradient represent the *sensitivity* of the cost functional $\mathcal{J}(\psi_b)$ with respect to the boundary control ψ_b and can be used in combination with algorithm (73) to "design" an optimal Prandtl–Batchelor vortex. The derivation shown is intended only to illustrate the general framework, and work is ongoing to use this approach to solve an actual "vortex design" problem. Exhaustive analysis of this problem together with computational results are going to be presented in a forthcoming paper [133]. Finally, we note that owing to the presence of Dirac measures on the vortex boundary ∂A, adjoint system (99) may be nontrivial to solve numerically.

7. Summary, Conclusions and Discussion of Future Perspectives

In this final Section we summarize the main themes discussed in this review. The utility of point vortex models for solution of flow control problems stems from the very fact that they offer a low–dimensional description of the flow system that preserves some of its key nonlinear features. As was illustrated with several examples in this paper, such simplified "reduced–order" models often lend themselves to an explicit design of controllers and estimators which can be carried out using rigorous methods of the modern control theory, an impossible task for most problems described by the full Navier–Stokes system [12]. A good example was offered in Section 4.2 where a fairly complete analysis and design of a linear control approach could be carried out for the Föppl system [108, 63, 110, 111]. Control algorithms developed using point vortex models are often subsequently employed to control "real" flows of viscous fluids, and we presented several examples illustrating this approach. As regards the analysis of flow control systems, point vortex models might be proposed as a simple paradigm for studying controllability and observability of flows. For example, the fact that the Föppl system with the cylinder rotation used as the actuation is uncontrollable, whereas the same system with the blowing and suction used as the actuation is controllable, might explain why the latter form of actuation tends to be more effective in many real applications. As regards the control synthesis, the use of low–dimensional vortex models bypasses the problems related to the numerical solution of the algebraic Riccati equation. This operator equation, whose solutions are needed in order to determine the feedback gains for optimal linear controllers and estimators, can be exceedingly difficult to solve for problems with a high dimension of the state space.

Our comparison of different controlled point vortex systems reveals certain generic behaviors. In several problems involving stabilization of unstable equilibria [98, 101, 108] the

trajectories of the controlled vortex systems would converge to circular orbits circumscribing the equilibrium. Rigorous mathematical analysis carried out in [110] showed that, at least for the Föppl system with a linear state feedback control, this orbit had the structure of a center manifold, and the stability of the system motion on this manifold had origins in the Hamiltonian structure of the point vortex system. While in other cases this has not been established rigorously, it is plausible that a center manifold structure may also be present in other systems in which such behavior was observed.

One area omitted in this review are applications of "vortex methods", understood as numerical techniques for certain classes of PDEs rather than "flow models", to solution of flow control problems formulated in a traditional manner, i.e., with no reference to vortex dynamics (see, e.g., [134, 135]).

We close this paper by commenting on some possible future research directions. We have seen evidence that solution of control problems for point vortex systems is now relatively well understood, so that problems of practical importance can actually be tackled, as was done for example in a recent experimental study [136]. In Section 6 we presented some initial developments concerning the control of Euler flows with finite 2D vorticity distributions. While specific cases have yet to be solved, a general mathematical framework required to handle such problems already exists. Work on this problem is underway and results will be reported in the near future. Another area of vortex dynamics where virtually no control problems have been formulated and solved in a systematic manner are 3D flows. The reason is that point vortices do not in fact have a simple 3D counterpart. If such 3D vortex models could be established, we anticipate that they would be amenable to treatment using control methods analogous to those described in this review in the context of 2D flows. Yet another area of vortex dynamics that remains a largely uncharted territory from the point of view of control are 2D flows with vorticity distributed along 1D objects (vortex sheets). Recently there have been some exciting new developments [47, 48, 49] concerning the mathematical modeling and computation of these flows, in addition to control–theoretic investigations [137]. Such vortex models are relevant for problems of animal propulsion, and in our opinion in the near future this area will be the stage for many interesting flow control problems. Given the nature of the vorticity support in such flows, we expect that solution of the resulting control problems will require shape–differential tools quite similar to those introduced in Section 6. From the point of view of the control theory, other promising, albeit mostly unexplored, topics include applications of nonlinear control methods [138, 139], especially methods of geometric control, dynamic programming methods based on the Hamilton–Jacobi–Bellmann equation as well as the Ensemble Kalman Filtering to vortex systems.

Acknowledgments

The author wishes to thank T. Bewley, S. Boatto, O. Cadot, T. Duriez, A. Elcrat, F. Gallizio, A. Iollo, M. Mahmood, K. Miller, D. Pelinovsky, J.-E. Wesfreid, and L. Zannetti for many stimulating discussions. The author also wishes to acknowledge generous financial support from NSERC–Discovery (Canada) and CNRS (France). Computational time for several

investigations reported in this article was provided by SHARCNET (Canada).

References

[1] Sontag E D 1998 *Mathematical Control Theory. Deterministic Finite-Dimensional Systems* Springer–Verlag

[2] Andrei N 2006 Modern Control Theory — A historical perspective *Studies in Informatics and Control* **10** 51–62

[3] Luenberger D G 1969 *Optimization by Vector Space Methods* Wiley

[4] Boyd S and Vandenberghe L 2004 *Convex Optimization* Cambridge University Press

[5] Nocedal J and Wright S J 2006) *Numerical Optimization* Springer

[6] Pontryagin L S, Boltyanskii V G, Gamkrelidze R V, and Mishchenko E F 1962 *The Mathematical Theory of Optimal Processes* Wiley

[7] Stengel R F 1994 *Optimal Control and Estimation* Dover Publications

[8] Lions J L. 1969 *Contrôle Optimal des Systèmes Gouvernés par des Equations aux Dérivées Partialles* (Dunod, Paris , English translation, Springer–Verlag, New York)

[9] Zabczyk J 1992 *Mathematical Control Theory: An Introduction* (Birkhäuser)

[10] Gunzburger M D 2003 *Perspectives in flow control and optimization* (SIAM, Philadelphia)

[11] Aamo O M and Krstic M 2002 *Flow Control by Feedback* (Springer)

[12] Bewley T R 2001 Flow control: new challenges for a new Renaissance *Progress in Aerospace Sciences* **37**, 21–58

[13] Kim J 2003 Control of turbulent boundary layers *Phys. Fluids* **15**, 1093–1105

[14] Kim J and Bewley T R 2007 A linear systems approach to flow control *Annual Review of Fluid Mechanics* **39**, 383–417

[15] Lumley J L and Blossey P N 1998 Control of turbulence *Annual Review of Fluid Mechanics* **30**, 311

[16] Rowley C W and Williams D R 2006 Dynamics and Control of High-Reynolds-Number Flow over Open Cavities *Annual Reviews of Fluid Mechanics* **30**, 251–276

[17] King R (Ed.) 2007 *Active Flow Control (Notes on Numerical Fluid Mechanics and Multidisciplinary Design)* (Springer)

[18] Chomaz J–M 2005 Global Instabilities in Spatially Developing Flows: Non–normality and Nonlinearity *Annual Reviews of Fluid Mechanics* **37**, 357–392

[19] Lauga E and Bewley T R 2004 Performance of a linear robust control strategy on a nonlinear model of spatially-developing flows *Journal of Fluid Mechanics* **512** 343–374.

[20] Lauga E and Bewley T R 2002 Modern control of linear global instability in a cylinder wake model *International Journal of Heat and Fluid Flow* **23** 671–677

[21] Aamo O M, Smyshlyaev A, and Krstic M 2005 Boundary control of the linearized Ginzburg–Landau model of vortex shedding *SIAM Journal of Control and Optimization* **43** 1953–1971

[22] Aamo O M, Smyshlyaev A, Krstic M, and Foss B 2007 Stabilization of a Ginzburg–Landau model of vortex shedding by output–feedback boundary control,*IEEE Transactions on Automatic Control* **52** 742–748

[23] Vainchtein D and Mezić I 2006 Vortex-based control algorithms *Lecture Notes in Control and Information Sciences* **330** (Springer)

[24] Helmholtz H 1858 Über Integrale der hydrodynamischen Gleichungen, welche den Wirbelbewegungen entsprechen *J. Reine Angew. Math.* **55** (1858) 25–55

[25] Truesdell C 1954 *The Kinematics of Vorticity* (Indiana University Press)

[26] Meleshko V V and Aref H 2007 A bibliography of vortex dynamics 1858–1956 *Advances in Applied Mechanics* **41** 197–292

[27] Lamb H 1932 *Hydrodynamics (*6^{th} *Edition)* (Cambridge University Press)

[28] Villat H 1933 *Mécanique des fluides* (Gauthier–Villars, Paris)

[29] Kochin N E, Kibel I A and Rose I W 1948 *Theoretical Hydrodynamics (in Russian)*, (Ogiz, Leningrad)

[30] Milne–Thompson L M 1955 *Theoretical Hydrodynamics* (MacMillan, London)

[31] Batchelor G K 1967 *An Introduction to Fluid Dynamics* (Cambridge University Press, Cambridge)
[32] Saffman P G 1992 *Vortex Dynamics* (Cambridge University Press, Cambridge)
[33] Newton P K 2001 *The N–Vortex Problem. Analytical Techniques* (Springer, New York)
[34] Boatto S and Crowdy D G 2006 Point vortex dynamics In *Encyclopedia of Mathematical Physics* Springer–Verlag
[35] Aref H 2007 Point vortex dynamics: A classical mathematics playground *Journal of Mathematical Physics* **28**, 065401
[36] Marchioro C and Pulvirenti M 1994 *Mathematical Theory of Incompressible Nonviscous Fluids* (Springer, New York)
[37] Majda A J and Bertozzi A L 2002 *Vorticity and Incompressible Flow* (Cambridge University Press, Cambridge)
[38] Rosenhead L 1932 The point vortex approximation of a vortex sheet *Proc. R. Soc. London Ser. A* **134**, 170–192
[39] Cottet G-H and Koumoutsakos P D 2000 *Vortex Methods: Theory and Practice* (Cambridge University Press)
[40] Batchelor G 1957 Steady laminar flow with closed streamlines at large Reynolds number *J. Fluid Mech.* **1**, 177-190
[41] Batchelor G 1957 A proposal concerning laminar wake behind bluff bodies at large Reynolds numbers *J. Fluid Mech.* **1**, 388-398
[42] Chorin A J 1994 *Vorticity and Turbulence* Springer
[43] Onsager L 1949 Statistical hydromechanics, *Nuovo Cimento* **6** (Suppl.) 279–287
[44] McWilliams J C 2006 *Fundamentals of Geophysical Fluid Dynamics* Cambridge University Press
[45] Saffman P G and Sheffield J S 1977 Flow over a Wing with an Attached Free Vortex *Studies in Applied Mathematics* **57**, 107–117
[46] Ringleb F O 1961 Separation control by trapped vortices. In: Lachmann G V (ed.), *Boundary Layer and Flow Control* **1** (Pergamon Press, Oxford), 265–294
[47] Hou T Y, Stredie V Ga and Wu T Y 2007 Mathematical modeling and simulation of aquatic and aerial animal locomotion *J. Comp. Phys.* **225**, 1603–1631
[48] Shukla R K and Eldredge J D 2007 An inviscid model for vortex shedding from a deforming body *Theor. Comput. Fluid Dyn.* **21** 343–368
[49] Xiong H and Kelly S D 2007 Self–Propulsion of a Deformable Joukowski Foil in a Perfect Fluid with Vortex Shedding (preprint)
[50] Aref H and Vainchtein D 1998 Asymmetric equilibrium patters of point vortices, *Nature* **392**, 769–770
[51] Gröbli W 1877 Spezielle Probleme über die Bewegung geradliniger paralleler Wirberfäden *Vierterjschr. Naturf. Ges. Zürich* **22** 37–82
[52] Aref H, Rott N and Thomann H 1992 Gröbli's solution of the three–vortex problem, *Annual Review of Fluid Mechanics* **24**, 1–20
[53] Lin C C 1943 *On the motion of vortices in two dimensions* The University of Toronto Press
[54] Crowdy D G and Marshall J S 2005 Analytical formulae for the Kirchhoff–Routh path function in multiply connected domains *Proc. Roy. Soc. A* **461**, 2477–2501
[55] Sychev V V, Ruban A I, Sychev V V and Korolev G L 1998 *Asymptotic Theory of Separated Flows* Cambridge University Press
[56] Wu J–Z, Ma H–Y and Zhou M–D 2006 *Vortex and Vortex Dynamics*, Springer
[57] Kirchhoff G 1876 *Vorlesungen über matematische Physik. Mechanik* Teubner, Leipzig
[58] Sadovskii V S 1971 Vortex regions in a potential stream with a jump of Bernoulli 's constant at the boundary *Appl. Math. Mech.* **35**, 729
[59] Pierrehumbert R T 1980 A family of steady, translating vortex pairs with distributed vorticity *J. Fluid Mech.* **99** 129–144
[60] Moore D W, Saffman P G and Tanveer S 1988 The calculation of some Batchelor flows: The Sadovskii vortex and rotational corner flow *Phys. Fluids* **31** 978–990
[61] Elcrat A, Fornberg B, Horn M and Miller K 2000 Some steady vortex flows past a circular cylinder *J.*

Fluid Mech. **409**, 13-27
[62] Föppl L 1913 Wirbelbewegung hinter einem Kreiscylinder *Sitzb. d. k. Bayer. Akad. d. Wiss.* **1**, 1-17 (English translation: Föppl L 1983 Vortex Motion Behind a Circular Cylinder *NASA Technical Memorandum* NASA TM–77015)
[63] Protas B 2006 Higher–order Föppl models of steady wake flows *Phys. Fluids* **18**, 117109
[64] Joukowski N E 1907 On annexed [bounded] vortices *Trudy Otd. Fiz. Nauk. Mosk. Obshch. Lyub. Estest. Antr. Etn.* **13** 12–25 (in Russian)
[65] Zannetti L 2007 Vortex equilibrium in flows past bluff bodies *J. Fluid Mech* **562** 151–171
[66] Turfus C 1993 Prandtl–Batchelor flow past a flat plate at normal incidence in a channel — inviscid analysis *J. Fluid Mech.* **249** 59–72
[67] Turfus C and Castro I P 2000 A Prandtl–Batchelor model of flow in the wake of a cascade of normal flat plates, *Fluid Dynamics Research* **26** 181–202
[68] Gallizio F 2004 Modello di Prandtl-Batchelor per il flusso normale ad una placca piana posta all'interno di un canale: studio numerico dell'esistenza e unicità della soluzione *Dissert. Tesi Laurea Ing. Aerosp.*, Politecnico di Torino, Torino, Italy
[69] Cox J 1973 The Revolutionary Kasper Wing *Soaring* **37** 20–23
[70] Huang M–K and Chow Ch–Y 1982 Trapping of a Free Vortex by Joukowski Airfoils *AIAA Paper* 82–4059
[71] The *VortexCell2050 project* funded by the European Commission within its FP6 Programme, contract number AST4–CT–2005–012139 (more information available at `www.vortexcell2050.org`)
[72] Bunyakin A V, Chernyshenko S I and Stepanov G Yu 1998 High–Reynolds–number Batchelor–model asymptotics of a flow past an aerofoil with a vortex trapped in a cavity *J. Fluid Mech.* **358** 283–297.
[73] Pullin D I 1984 A constant vorticity Riabouchinsky free streamlines flow *Quart. J. Math. Appl. Mech* **37** 619–631
[74] von Kármán Th 1954 *Aerodynamics. Selected Topics in the Light of their Historical Development* Cornell University Press, Ithaca
[75] Heisenberg W 1922 Die absoluten Dimensionen der Kármánschen Wirbelbewegung *Phys. Z.* **23** (1922) 363-366 (English translation: Heisenberg W 1923 Absolute Dimensions of Karman Vortex Motion *National Advosory Committee for Aeronautics — Technical Notes* **126**)
[76] Villat H 1929 La théorie de l'experience de M. Henri Bénard sur les tourbillons alternés dans une cuve limitée par deux parois fixes parallèles *Ann. Sci. de l'É.N.S.* **46** 259–281
[77] Aref H, Stremler M A and Ponta F L 2006 Exotic Vortex Wakes — Point Vortex Solutions *J. of Fluids and Struct.* **22** 929–940
[78] Tang S and Aubry N 1997 On the symmetry breaking instability leading to vortex shedding *Physics of Fluids* **9**, 2550–2561
[79] Smith A C 1973 On the stability of Föppl vortices *J. Appl. Mech* **40**, 610
[80] Cai J, Liu F and Luo S 2001 Stability of a Vortex Pair behind Two–Dimensional Bodies *AIAA Paper* 2001–2844
[81] de Laat T W G and Coene R 1995 Two–dimensional vortex motion in the cross–flow of a wing–body configuration *J. Fluid Mech.* **305**, 93–109
[82] Elcrat A, Fornberg B and Miller K 2005 Stability of vortices in equilibrium with a cylinder *J. Fluid Mech.* **544**, 53–68
[83] Tordella D 1995 Nonsteady stability of the flow around the circle in the Föppl model *Quart. Appl. Math*, **53**, 683
[84] Shashikanth B N, Marsden J E, Burdick J W and Kelly S D 2002 The Hamiltonian structure of a two–dimensional rigid circular cylinder interacting dynamically with N point vortices *Physics of Fluids* **14**, 1214
[85] Vainchtein D and Mezić I 2002 Control of a Vortex Pair using a weak external flow *Journal of Turbulence* **3**
[86] Vainchtein D and Mezić I 2004 Optimal control of a co–rotating vortex pair: averaging and impulsive control *Physica D* **192**, 63–82
[87] Khalil H K 2002 *Nonlinear Systems* Prentice–Hall

[88] Tadmor G 2004 Observers and Feedback Control for a Rotating Vortex Pair *IEEE Transactions on Control Systems Technology* **12**, 36–51
[89] Coron J–M 2007 *Control and Nonlinearity* American Mathematical Society
[90] Péntek Á, Kadtke J B and Toroczkai Z 1996 Stabilizing chaotic vortex trajectories: an example of high–dimensional control *Phys. Lett. A* **224** 85–92
[91] González–Miranda J M 2004 *Synchronization and control of chaos: an introduction for scientists and engineers* Imperial College Press
[92] Ott E, Grebogi C and Yorke J A 1990 Controlling Chaos *Phys. Rev. Lett.* **64** 1196–1199
[93] Noack B R, Mezić I, Tadmor G and Banaszuk A 2004 Optimal mixing in recirculation zones *Phys. Fluids* **16**, 867-888
[94] Coller B D, Noack B R, Narayanan S, Banaszuk A and Khibnik A I 2000 Reduced–Basis Model for Active Separation Control in a Planar Diffuser Flow, *AIAA Paper* 2000–2562
[95] Pastoor M, King R, Noack B R, Dillmann A and Tadmor G 2003 Model–Based Coherent–Structure Control of Turbulent Shear Flows Using Low–Dimensional Vortex Models *AIAA Paper* 2003–4261
[96] Cortelezzi L, Leonard A and Doyle J C 1994 An example of active circulation control of the unsteady separated flow past a semi–infinite plate *J. Fluid Mech.* **260** 127–154
[97] Cortelezzi L 1996 Nonlinear feedback control of the wake past a plate with a suction point on the downstream wall *J. Fluid Mech.* **327** 303–324
[98] Cortelezzi L, Chen Y–C and Chang H–L 1997 Nonlinear feedback control of the wake past a plate: From a low–order model to a higher–order model *Phys. Fluids* **9** 2009–2022
[99] Brown C E and Michael W H 1954 Effect of leading edge separation on the list of a delta wing *J. Aero. Sci* **21** 690–694
[100] Anderson C R, Chen Y–C and Gibson J S 2000 Control and Identification of Vortex Wakes *J. Dyn. Sys. Meas. Control — Trans, ASME* **122** 298–305
[101] Zannetti L and Iollo A 2003 Passive Control of the Vortex Wake Past a Flat Plate at Incidence *Theoret. Comput Fluid Dynamics* **16** 211–230
[102] Luithardt H H, Kadtke J B and Pedrizzetti G 1994 Chaotic capture of vortices by a moving body. II. Bound pair model *Chaos* **6** 681–691
[103] Kadtke J, Péntek Á and Pedrizzetti G 1995 Controlled capture of a continuous vorticity distribution *Phys. Lett. A* **204** 108–114
[104] Chernyshenko S I 1995 Stabilization of trapped vortices by alternating blowing suction *Phys Fluids* **7** 802–807
[105] Péntek Á, Kadtke J B Pedrizzetti G 1998 Dynamical control for capturing vortices near bluff bodies *Phys. Rev. E* **58** 1883–1898
[106] Tang S and Aubry N 2000 Suppression of vortex shedding inspired by a low–dimensional model *J. Fluids and Struct.* **14**, 443–468
[107] Li F and Aubry N 2003 Feedback control of a flow past a cylinder via transverse motion *Physics of Fluids* **15**, 2163–2176
[108] Protas B 2004 Linear Feedback Stabilization of Laminar Vortex Shedding Based on a Point Vortex Model *Physics of Fluids* **16**, 4473–4488
[109] Protas B and Wesfreid J–E 2003 On the Relation Between the Global Modes and the Spectra of Drag and Lift in Periodic Wake Flows *Les Comptes Rendus de l'Académie des sciences, Série IIB - Mécanique* **331**, 49–54
[110] Protas B 2007 Center Manifold Analysis of a Point-Vortex Model of Vortex Shedding with Control *Physica D* **228** 179–187
[111] Protas B 2007 Vortex models for feedback stabilization of wake flows In R. King (Ed.) *Active Flow Control (Papers contributed to the Conference "Active Flow Control 2006", Berlin, Germany, September 27–29, 2006)*, Notes on Numerical Fluid Mechanics and Multidisciplinary Design, Springer
[112] Datta B 2003 *Numerical Methods for Linear Control Systems* Academic Press
[113] Zhou K, Doyle J C and Glover K 1995 *Robust and Optimal Control* Prentice Hall
[114] Wiggins S 1990 *Introduction to Applied Nonlinear Dynamical Systems and Chaos* Springer

[115] Carr J 1981 *Applications of Centre Manifold Theory* Springer
[116] Protas B and Wesfreid J–E 2002 Drag Force in the Open–Loop Control of the Cylinder Wake in the Laminar Regime *Phys. Fluids* **14**, 810–826
[117] Ma Z and Shashikanth B N 2006 Dynamics and control of the system of a 2–D rigid circular cylinder and point vortices *Proceedings of the 2006 American Control Conference, Minneapolis, Minnesota, USA, June14-16, 2006*, 4927–4932
[118] Shashikanth B N 2007 Symmetry reduction and control of the dynamics of a 2-D rigid circular cylinder and a point vortex: vortex capture and scattering *European Journal of Control* (to appear)
[119] Borisov A V, Mamaev I S, and Ramodanov S M 2007 Dynamic interaction of point vortices and a two-dimensional cylinder *J. Math. Phys.* **48**, 065403
[120] Iollo A and Zannetti L 2001 Trapped vortex optimal control by suction and blowing at the wall *European Journal of Mechanics B – Fluids* **20** 7–24
[121] Iollo A and Zannetti L 2000 Optimal Control of a Vortex Trapped by an Airfoil with a Cavity *Flow, Turbulence and Combustion* **65** 417–430
[122] Nocedal J and Wright S 2000 *Numerical Optimization* Springer
[123] Tadmor G and Banaszuk A 2002 Observer–Based Control of Vortex Motion in a Combustor Recirculation Region *IEEE Transactions on Control Systems Technology* **10**, 749–755
[124] Ide K and Ghil M 1997 Extended Kalman filtering for vortex systems: I. Methodology and point vortices *Dyn. Atmos. Oceans* **27** 301–332
[125] Ide K, Kuznetsov L and Jones C K R T 2002 Lagrangian data assimilation for point vortex system *Journal of Turbulence* **3** 053
[126] Deem G S and Zabusky N J 1978 Vortex waves: Stationary V–states, interactions, recurrence, and breaking *Phys. Rev. Lett.* **40** 859–863
[127] Friedland L 1999 Control of Kirchhoff vortices by a resonant strain *Physical Review E* **59** 4106–4111
[128] Friedland L and Shagalov A G 2000 Resonant formation and control of 2D symmetric vortex waves *Physical Review Lett.* **85** 2941–2944
[129] Friedland L and Shagalov A G Emergence of nonuniform V–states by synchronization *Physics of Fluids* **14** 3074–3086
[130] Ottino J M 1995 *The kinematics of mixing: stretching, chaos and transport*, Cambridge University Press
[131] Sokolowski J and Zolésio J–P 1992 *Introduction to shape optimization: shape sensitivity analysis* Springer
[132] Berger M S 1977 *Nonlinearity and Functional Analysis* Academic Press
[133] Protas B 2008 "Vortex Design Problem" (in preparation)
[134] Protas B and Styczek A 2002 Optimal Rotary Control of the Cylinder Wake in the Laminar Regime *Physics of Fluids* **14** 2073–2087
[135] Protas B 2002 On the "Vorticity" Formulation of the Adjoint Equations and its Solution Using Vortex Method *Journal of Turbulence* **3** 048
[136] Pastoor M, Henning L, Noack B R, King R, and Tadmor G 2008 Feedback shear layer control for bluff body drag reduction *Journal of Fluid Mechanics* (accepted for publication)
[137] Kelly S 2007 The Mechanics and Control of Driftless Swimming (preprint)
[138] Aamo O M and Krstic M 2004 Feedback control of particle dispersion in bluff body wakes *International Journal of Control* **77** 1001–1018
[139] Yuan C C, Krstic M, and Bewley T 2004 Active control of jet mixing *IEE Proceedings: Control Theory and Applications* **151** 763–772